# Amplification of Elementary Surface Reaction Steps on Transition Metal Surfaces using Liquid Crystals: Dissociative Adsorption and Dehydrogenation

Huaizhe Yu<sup>†,+</sup>, Tibor Szilvási<sup>‡,+</sup>, Kunlun Wang<sup>#</sup>, Jake I. Gold<sup>‡</sup>, Nanqi Bao<sup>†</sup>, Robert J. Twieg<sup>#</sup>, Manos Mavrikakis\*,<sup>‡</sup> and Nicholas L. Abbott\*,<sup>†</sup>

†Robert Frederick Smith School of Chemical and Biomolecular Engineering, Cornell University, 1 Ho Plaza, Ithaca, New York 14853, United States

<sup>‡</sup>Department of Chemical and Biological Engineering, University of Wisconsin-Madison, 1415 Engineering Drive, Madison, Wisconsin 53706, United States

ABSTRACT: Elementary reaction steps, including adsorption and dissociation, of a range of molecular adsorbates on transition metal surfaces have been elucidated in the context of chemical catalysis. Here we leverage this knowledge to design liquid crystals (LCs) supported on ultrathin polycrystalline gold films (predominant crystallographic face is (111)) that are triggered to undergo orientational transitions by dissociative adsorption and dehydrogenation reactions involving chlorine and carboxylic acids, respectively, thus amplifying these atomic-scale surface processes *in situ* into macroscopic optical signals. We use electronic structure calculations to predict that 4'-n-pentyl-4-biphenylcarbonitrile (5CB), a room temperature nematic LC, does not bind to Au(111) in an orientation that changes upon dissociative adsorption of molecular chlorine, a result validated by experiments. In contrast, 4-cyano-4-biphenylcarboxylic acid (CBCA) is calculated to bind strongly to Au(111) in a perpendicular orientation via dehydrogenation of the carboxylic acid group, which we confirmed using polarization-modulation infrared reflection-absorption spectroscopy. A maximum coverage of 0.07 monolayer of CBCA on the gold surface is sufficient to cause a perpendicular orientation of the LC. Dissociative adsorption of Cl<sub>2</sub> gas on the gold surface, resulting in 0.5 monolayer coverage, displaces CBCA from Au(111) and thus triggers a strikingly visible change in orientation of the LC. Infrared spectroscopy established the orientation of adsorbed CBCA to be parallel to the Cl covered surface, with the COOH plane perpendicular to the surface, as predicted by first principles calculations. These results demonstrate the use of first-principles calculations and transition metal surfaces to design LCs that report *in situ* targeted atomic-scale surface processes.

#### INTRODUCTION

The elucidation of processes that amplify specific atomic-scale events into the macroscopic scale defines one of the central scientific challenges because such processes can provide fundamental insights into nanoscopic events<sup>1,2</sup> as well as form the basis of technologically useful phenomena that enable the design of programmable, stimuli-responsive materials.<sup>3–5</sup> Liquid crystals (LCs), which are fluid phases within which molecules exhibit preferred orientations, are characterized by remarkable cooperative behaviors that allow information encoded in sub-molecular-level interactions to be amplified into the optical scale (micrometer-scale). 6-10 For example, the dissolution of chiral molecular solutes within a LC phase can give rise to the appearance of helical organizations of the LC on the micrometer-scale (so-called cholesteric or blue phase LCs). 11,12 Alternatively, intermolecular interactions, such as hydrogen bonding or metal cation-ligand coordinating interactions, between LCs and adsorbates presented at surfaces can lead to orientations of LCs that propagate over distances of micrometers from the surfaces. 10,13-15 Interestingly, recent studies have also demonstrated

that control of the micrometer-scale structure of LCs can be used to transmit information from the microscale down into the nano-scale via the introduction of topological defects into  $LCs.^{16-18}$ 

One of the key barriers to development of a more complete understanding of how information encoded in Angstrom-level molecular interactions at interfaces leads to micrometer-scale ordering of LCs is the paucity of robust yet atomically-defined surfaces on which relevant physical and chemical interactions of LCs can be studied. 19-21 This challenge is not limited to studies of the ordering of LCs at surfaces but is faced by broad communities in the chemical sciences investigating both organic and inorganic supramolecular assemblies at interfaces. <sup>22–26</sup> Of particular relevance to the study reported in this paper, over the past decade, the atomic-level understanding of elementary reaction steps on transition metals and metal-oxides surfaces has resulted in important advances in heterogeneous catalysis. 27-29 This knowledge has led to the rational design of catalysts and functional photonic materials, and simultaneously advanced our understanding of fundamental interfacial processes. 30-32 In this

<sup>\*</sup>Department of Chemistry and Biochemistry, Kent State University, 1175 Risman Drive, Kent, Ohio 44242, United States

paper, we describe a first effort to leverage this knowledge into fundamental insights into atomic-scale interfacial processes that can be amplified into micrometer-scale ordering transitions in LCs.

The study reported in this paper is focused on noble metal surfaces (Au(111)) and the interaction of molecular chlorine, carboxylic acids or nitrile groups with this surface. Our focus on chlorine gas (Cl<sub>2</sub>) was motivated by the observation that Cl<sub>2</sub> dissociatively adsorbs on Au(111).<sup>33</sup> Previous ultra-high vacuum (UHV) studies have shown that Cl<sub>2</sub> adsorption on Au(111) causes a herringbone surface reconstruction<sup>34</sup> and formation of a  $(\sqrt{3} \times \sqrt{3})R30^{\circ}$  overlayer of chlorine atoms that is stable up to temperatures as high as 600 K.33 Carboxylic acids were selected as a second class of adsorbates to study because they can participate in deprotonation, dehydrogenation and other reactions on Au(111) surfaces. 35-39 Specifically, scanning tunneling microscopy measurements have revealed that carboxylic acids form hydrogen bonded dimers on clean Au(111)<sup>39-41</sup> but, in the presence of pre-adsorbed oxygen atoms, dehydrogenation reactions occur readily<sup>39</sup>. Additionally, decomposition of formic acid has been extensively studied using experimental<sup>42,43</sup> and theoretical approaches on Au(111)<sup>43,44</sup>. Our study also involves the interaction of nitrile-functionalized molecules with Au(111), an interaction that has been shown to depend on several factors such as adjacent functional groups<sup>45</sup> or electrical potential of the Au<sup>46,47</sup>.

In this paper, we combine and develop further our understanding of the above-described atomic scale processes occurring on Au(111) through a combination of predictive first-principles electronic structure calculations and experiments. We leverage that understanding to identify interfacial designs that couple the dissociative adsorption of chlorine gas to orientational transitions involving carboxylic acid-containing LCs on Au surfaces. We find that LC orientational transitions occur with dynamics and sensitivity to concentrations of gaseous Cl<sub>2</sub> that appear promising as the basis of new designs of wearable sensors for measurement of human exposure to Cl<sub>2</sub> gas. <sup>48</sup> We also show that the optical response of the LC is selective to Cl<sub>2</sub> over a range of other gases including N<sub>2</sub>, dimethyl methylphosphonate, ammonia, ethylene oxide, and formaldehyde.

#### THEORETICAL AND EXPERIMENTAL METHODS

Computational methods. All calculations were performed using Density Functional Theory, as implemented in the Vienna Ab initio Simulation Package (VASP) code. 49,50 Projector augmented wave potentials were used to describe the electron-ion interactions, 51,52 and the exchange-correlation functional was described by the generalized gradient approximation (GGA-PBE).<sup>53</sup> Dispersion corrections were used in all calculations employing Grimme's D3 empirical dispersion correction scheme with zero damping.<sup>54</sup> The electron wave function was expanded using plane waves with an energy cutoff of 400 eV in geometry optimization. The Brillouin zone (BZ) of Au(111) was sampled using  $(4 \times 4 \times 1)$ ,  $(3 \times 3 \times 1)$ , and  $(1 \times 3 \times 1)$   $\Gamma$ -centered Monkhorst-Pack k-point mesh<sup>55</sup> in the case of  $(3\times3)$ ,  $(4\times4)$ , and  $(8\times4)$ unit cell calculations, respectively. In all calculations, the Methfessel-Paxton smearing method<sup>56</sup> was used with 0.1 eV smearing. Structures were relaxed until the Hellmann-Feynman forces acting on each atom were less than 0.02 eV Å-1. Transition state calculations were carried out with the climbing image nudged elastic band (CI-NEB) method using seven intermediate images and the same other settings described above.<sup>57</sup>

The calculated Au lattice constant of 4.12 Å is in good agreement with the experimental value of 4.08 Å.58 The gold surface was modeled using the most stable (111) facet with a four-layer slab. The two bottom layers of the slab were fixed in their bulk positions, while the two top layers of Au atoms were relaxed in all calculations. The Au slab images were separated by a distance of 25 Å to ensure that adsorbed benzonitrile (PhCN) molecules, which were used as surrogates of 4'-n-pentyl-4-biphenylcarbonitrile (5CB),<sup>59</sup> did not decrease the vacuum layer separating the images below 15 Å, even in the case of a perpendicular orientation of the PhCN adsorbates. Dipole correction was used to eliminate residual interaction between images through the vacuum layer. To allow for parallel adsorbed states of PhCN, a (4×4) unit cell was used to model Au(111). The binding of other analytes (N2, dimethyl methylphosphonate, ammonia, ethylene oxide, and formaldehyde) was also evaluated in a  $(4\times4)$  unit cell with one analyte in the simulation box. The binding energy (BE) of an adsorbate is defined by BE = Etotal - Esubstrate - Egas phase adsorbate where Etotal is the total energy of the entire adsorbate-slab system, E<sub>substrate</sub> is the total energy of the clean Au(111) slab, and Egas-phase adsorbate is the total energy of the isolated adsorbate in the gas phase. By this definition, a more negative BE value reflects a stronger binding to the surface. To assess Cl coverage on Au under experimentally relevant conditions, we calculated a phase diagram for Cl adsorption on Au(111) over a wide temperature and pressure range. 60-<sup>62</sup> Additional details can be found in Supporting Information

Materials. The precursor 4-bromobenzoic acid was purchased from Synquest Laboratories (Alachua, FL). 4-cyanophenylboronic acid was purchased from Combi-Blocks (San Diego, CA). PdCl<sub>2</sub> for the synthesis of Pd(PPh<sub>3</sub>)<sub>4</sub> was bought from Pressure Chemical (Pittsburgh, PA). Potassium carbonate and 1,4-dioxane were bought from Alfa Aesar (Ward Hill, MA). Methanol was purchased from VMR (West Chester, PA). Ethanol, hydrochloric acid (37%) and sulfuric acid (98%) were bought from Sigma-Aldrich (Milwaukee, WI). Diethyl ether and t-BuONa were purchased from Acros. Titanium (99.999%) and gold (99.999%) were purchased from Advanced Materials (Spring Valley, NY). Methanol and Fischer's Finest glass slides were purchased from Fischer Scientific (Pittsburgh, PA). Silicon wafers were purchased from Silicon Sense (Nashua, NH). Cl<sub>2</sub> in nitrogen gas (purity of Cl<sub>2</sub> is 99.9% and purity of nitrogen is 99.999%) at a concentration of 10 ppm and nitrogen gas (99.998% purity) were obtained from Airgas (Radnor Township, PA)) and used as received. All chemicals and solvents were of analytical reagent grade and were used as received without any further purification. Fiber spacers with 5 µm-diameter were purchased from EM industries, Inc (Hawthorne, NY).

**Synthesis.** The syntheses of 4'-cyanobiphenyl-4-carboxylic acid (CBCA), 4'-cyanobiphenyl-4-carboxylic methyl ester (CBCM) and sodium 4'-cyanobiphenyl-4-carboxylate (CBCNa) are summarized in Scheme 1 and additional details can be found in SI.

(a) NC 
$$C_{g}H_{11}$$
 5CB NC  $COOH$  CBCA

NC  $COOMe$  CBCM NC  $COONe$  CBCM NC  $COONe$  CBCNa

(b) NC  $COOH$   $COOH$ 

**Scheme 1.** (a) Molecular structure of 4'-n-pentyl-4-biphenyl-carbonitrile (5CB), 4-cyano-4-biphenylcarboxylic acid (CBCA), 4-cyano-4-biphenylcarboxylic methyl ester (CBCM) and 4-cyano-4-biphenylcarboxylate sodium (CBCNa) (b) Synthesis of CBCA, CBCM and CBCNa.

Cleaning of glass substrates. Glass microscope slides were cleaned according to published procedures  $^{63}$  using an acidic piranha solution [70:30 (% v/v)  $\rm H_2SO_4$  (70%): $\rm H_2O_2$  (30%)]. Piranha is extremely corrosive, potentially explosive and should not be exposed to organic material under any circumstances.  $^{64}$  Briefly, the glass slides were immersed in a piranha bath at 60-80  $^{\circ}$  C for at least 1 h and then rinsed in running deionized water for 2-3 mins. The slides were then immersed in basic piranha solution [70:30 (%v/v) KOH (45%): $\rm H_2O_2$  (30%)] and heated to between 60 and 80  $^{\circ}$  C for at least 1 h. Finally, the slides were rinsed sequentially in deionized water, ethanol, and methanol, and then dried under a stream of nitrogen. The clean slides were stored in a vacuum oven at 110  $^{\circ}$  C overnight. All other glassware was cleaned prior to use.

**Preparation of Substrates for Anchoring and Anchoring Transition Studies.** Semitransparent films of gold with thicknesses of 200 Å were deposited onto piranha-cleaned glass slides mounted on a fixed holder within an electron-beam evaporator (VEC-3000-C manufactured by Tekvac Industries, Brentwood, NY). A layer of titanium (thickness 20 Å) was used to promote adhesion between the glass microscope slides and the films of gold. The rates of deposition of both gold and titanium were 0.2 Å/s. The pressure in the evaporator was maintained below  $3 \times 10^{-6}$  Torr before and during the deposition.

Preparation of Substrates for X-Ray Photoelectron and Infrared Spectroscopy. Substrates used for the infrared (IR) and X-ray photoelectron spectroscopy (XPS) were prepared by sequential deposition of 100 Å of titanium and 1000 Å of gold onto silicon wafers. The gold-coated silicon wafers were then cut to 15 mm  $\times$  30 mm pieces and cleaned under a gaseous stream of nitrogen. For IR studies, 100  $\mu L$  of 2 mM CBCA in ethanol was spin coated onto each gold-coated silicon wafer at 3000 rpm for 30s. For XPS, the slides were exposed to gaseous 1 ppm Cl<sub>2</sub> for 15 mins.

Characterization of Orientations of LCs in Optical Cells. We fabricated optical cells from two gold-coated glass slides that were aligned facing each other and spaced apart using a glass spacer with a diameter of 5  $\mu$ m. Next, 2  $\mu$ L of LCs, heated to form an isotropic phase (35 °C < T < 40 °C), was drawn into the cavity between the two surfaces of the optical cell by capillarity. The optical appearance of the resulting LC film was characterized by using an Olympus BX-60 polarizing light micro-

scope in transmission mode (Olympus, Japan). Conoscopic imaging of the LC films was performed by inserting a Bertran lens into the optical path.<sup>65</sup>

**Ellipsometry.** The optical thicknesses of films of CBCA, CBCM and CBCNa deposited by spin-coating onto gold films were measured using a Gaertner LSE ellipsometer at a wavelength of 632.8 nm and an angle of incidence of  $70^{\circ}$ . The deposited films were assumed to have refractive indices of n = 1.6.66

Preparation of Micrometer-Thick Films of LC with Free Surfaces. An 18  $\mu m$ -thick copper-coated transmission electron microscopy (TEM) grid (Electron Microscopy Sciences, Hatfield, PA) was placed onto the surface of a semitransparent gold film. The TEM grids defined square pores with lateral dimensions of 285  $\mu m$ . 0.1  $\mu L$  of 5CB was deposited into each TEM grid using a glass capillary. The excess LC was removed from the grids by wicking the LC into an empty capillary tube.

Anchoring Transitions Induced by Cl<sub>2</sub>. LC samples hosted within TEM grids supported on gold films were exposed to a stream of nitrogen containing Cl<sub>2</sub> within a flow cell that was constructed to direct the gaseous flow across the LC samples while permitting observation of the samples through a polarized-light microscope (CH40, Olympus, Melville, NY). A detailed description of the flow cell can be found in a prior publication.<sup>67</sup> The stream of gas containing Cl<sub>2</sub> was generated from a certified cylinder containing 10 ppm Cl<sub>2</sub> in nitrogen, and diluted to using nitrogen to 1 ppm (see Materials for purity). The flow rate of gas through the flow cell was controlled to be 1000 mL/min using a series of rotameters (Aalborg Instruments & Controls, Inc., Orangeburg, NY).

**X-ray Photoelectron Spectroscopy (XPS).** X-ray photoelectron spectroscopy was performed with a Perkin-Elmer PhiX 5400 spectrometer. The X-ray source was Mg K $\alpha$ , and the scanning window was 2mm  $\times$  1 mm. Survey scans were performed for 10 cycles with a pass energy of 89.45 eV to identify elements present on the surface. The survey scan was then followed by element-specific acquisitions for Cl at 198.5 eV for twenty cycles.<sup>68</sup> The major peak was Cl (2p).

**Fourier Transform Infrared Spectroscopy (FTIR).** Transmission IR measurements were performed using a Bruker Vector 33 FTIR spectrometer (Bruker Optics Inc, Billerica, MA, USA). For each sample, 32 scans were acquired at a resolution of 5 cm<sup>-1</sup>. The data obtained was processed and plotted using OPUS software.

Fourier Transformed Polarization-Modulation Infrared Reflectance Absorbance Spectroscopy (PM-IRRAS). IR spectra of CBCA, CBCM and CBCNa films deposited onto gold-coated silicon wafers were obtained using a Nicolet Magna-IR 860 FT-IR spectrometer with a photoelastic modulator (PEM-90, Hinds Instruments, Hillsboro, OR), synchronous sampling demodulator (SSD-100, GWC Technologies, Madison, WI), and a liquid N<sub>2</sub>-cooled mercury cadmium telluride (MCT) detector. All spectra (1000-4000 cm<sup>-1</sup>) were recorded at an incident angle of 83° with the modulation centered at either 2200 cm<sup>-1</sup> or 1500 cm<sup>-1</sup>. For each sample, 1000 scans were taken at a resolution of 4 cm<sup>-1</sup>. Data were collected as differential reflectance vs wavenumber, and spectra were normalized and converted to absorbance units via the method outlined in Frey et al.<sup>69</sup>

#### RESULTS AND DISCUSSION

Influence of atomic Cl adsorbates on the orientations of nitrile-containing LCs on Au(111). Past studies have demonstrated that Cl<sub>2</sub> undergoes dissociative adsorption on Au(111) surfaces.<sup>34</sup> Our initial calculations and experiments sought to determine if nitrile-containing LCs bind to Au(111) surfaces in orientations that depend on whether or not the Au(111) surfaces are decorated with a bound Cl overlayer. In the absence of bound Cl, our simulations revealed that PhCN (surrogate for 5CB) aligns parallel to the surface in the most stable coordination mode (Figure 1, Table 1 and S2). In this preferred orientation, the interaction between the PhCN and the surface is dominated by dispersion interactions (Table 1). A feature of this binding mode is that the phenyl ring lies above a hollow site in the most stable structure, although we note that the energy difference between multiple stable minima is small (<0.05 eV). Similar conclusions have been reached in prior computational chemistry studies of benzene adsorption on Au(111). 70 As a result of the parallel binding mode, we predicted that nematic phases formed from 5CB would likely adopt a parallel orientation on Au(111) surfaces. We also predicted that the presence of bound Cl would likely not change the parallel orientation of nematic 5CB as additional calculations revealed that Cl chemisorption on the Au(111) surface did not interfere with the physisorption of PhCN in the parallel orientation (Figure S3). We validated the above-described computational predictions by experiment. Briefly, we determined that the orientation of 5CB on polycrystalline Au films (predominant crystallographic face is Au(111) is parallel to the surface (see Figure S4a and S5a), and that the orientation does not change when Cl is bound (Figure S5b). These preliminary results guided our subsequent efforts, as described below, to identify functional groups that could be incorporated into LCs and used to trigger the LCs to undergo orientational transitions upon dissociative adsorption of Cl<sub>2</sub> gas on Au(111) surfaces.

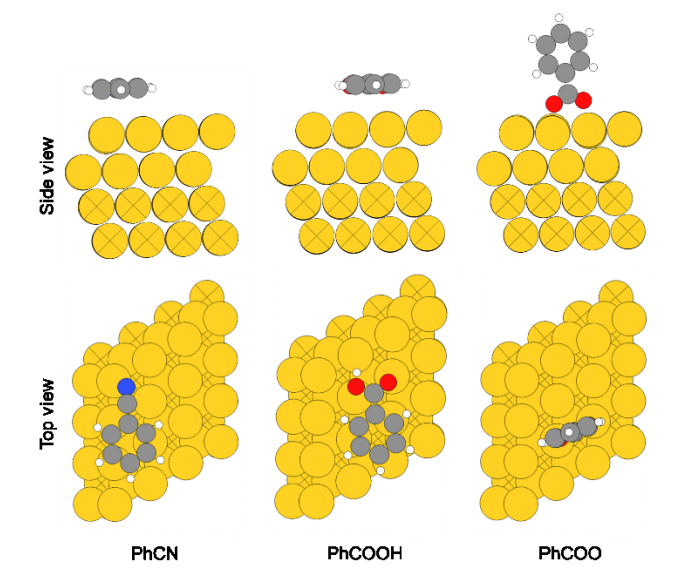


**Figure 1.** Cross section (top row) and top view (bottom row) for the energetically preferred orientations of PhCN, PhCOOH and PhCOO on Au(111). White, grey, blue, red, and yellow colors indicate H, C, N, O, Au atoms, respectively. Crossed atoms were not allowed to relax during geometry optimization.

**Table 1.** Calculated binding energy of adsorbates on clean Au(111) with orientations parallel or perpendicular to the gold surface in the (4x4) unit cell (Figure 1 and Figure S2). Most stable state for each species is in bold. All energies are in eV. Binding energy is defined relative to the energy of the identical species in the gas-phase. Calculated gas phase H-H, H-Cl, and O-H bond dissociation energies for H<sub>2</sub>, HCl, and PhCOOH are 4.53, 4.73, and 4.99 eV, respectively. Coverage is given in units of monolayers (ML).

Molecule	Parallel	Perpendicular	Coverage
PhCN	-0.91	-0.31	1/16
PhCOOH	-0.93	-0.36	1/16
PhCOO	-2.27	-2.50	1/16
PhCOONa	-1.01	-0.51	1/16
PhCOOMe	-1.08	-0.42	1/16
Н	-2.11		1/16
Cl	-2.70		1/16
Cl	-2.30		1/2

Interactions of aromatic carboxyl, carboxylate ester and carboxylate groups with Au(111) surfaces. Guided by the results described above, and prior reports of the various modes of interaction of carboxylic acid groups with Au(111) surfaces (see Introduction), we carried out first-principles calculations to gain insight into the interactions of the model compounds PhCOOH, PhCOO, PhCOONa and PhCOOMe with Au(111). Specifically, we determined their energetically preferred structures (Figure 1, Table 1 and S2). Similar to PhCN, we found that PhCOOH, PhCOONa, and PhCOOMe align parallel to the Au surface in the most stable adsorbed state (Figure 1, Table 1 and S2 due to dispersion interactions (Table 1). Interestingly, for PhCOO, however, a perpendicular orientation (relative to the gold surface) was predicted to be energetically favored (-2.50 eV, Figure 1 and Table 1). This preferred orientation is caused by strong binding of the O atoms in PhCOO to the top sites of the Au(111) surface. Because the O-O distance within PhCOO is only 2.11 Å while the Au-Au distance on the Au(111) surface is 2.91 Å, binding of PhCOO through the two O atoms occurs with the O atoms slightly displaced from the top of each Au atom, in agreement with earlier reports<sup>71</sup>.

The calculations in Table 1 led us to predict that the different potential modes of interaction of aromatic carboxylic acids and their derivatives with Au(111) surfaces may result in distinct orientations of the adsorbates and orientations of LCs. To explore these predictions, we synthesized CBCA. For use in control experiments, we also synthesized CBCM (acid converted to ester) and CBCNa (acid converted to sodium salt). By using differential scanning calorimetry (DSC) and polarized light microscopy, we determined that CBCA exhibited a nematic phase from 268 to 315 °C and decomposed at higher temperatures (see

Figure S6 and S7 for DSC and polarized light microscopy, respectively). In contrast, CBCM and CBCNa did not exhibit nematic phases in pure forms between 25 to 300 °C. Accordingly, to create nematic phases at room temperature, we mixed CBCA, CBCM or CBCNa with 5CB which, as described above, binds weakly and, alone, gives rise to planar anchoring on Au(111) surfaces.<sup>21</sup>

We characterized the orientations of LC mixtures containing 0.1 mol% of CBCA, CBCM or CBCNa in 5CB on gold films using polarized light microscopy (see Methods). We performed these measurements using vacuum-deposited polycrystalline Au films (predominately Au(111)) on borosilicate substrates. 72,73,74 Significantly, we measured the CBCA-5CB mixture to assume a homeotropic orientation on the gold films, whereas the CBCM-5CB and CBCNa-5CB mixtures assumed parallel orientations (Figure 2a-c). To further support the interpretation that the interaction of CBCA with Au is responsible for the homeotropic orientation of nematic CBCA-5CB, the mixture was deposited onto borosilicate surfaces (no gold) and the surfaces of silicon wafers covered with a native oxide, both which gave planar orientations of the LC (Figure S4b and S4c). Furthermore, when gold was deposited onto the silicon wafer with the native oxide, the CBCA-5CB mixture assumed a homeotropic orientation (Figure S4d). Overall, these initial results are consistent with the interaction between CBCA and gold giving rise to the homeotropic orientation of the CBCA-5CB mixture.

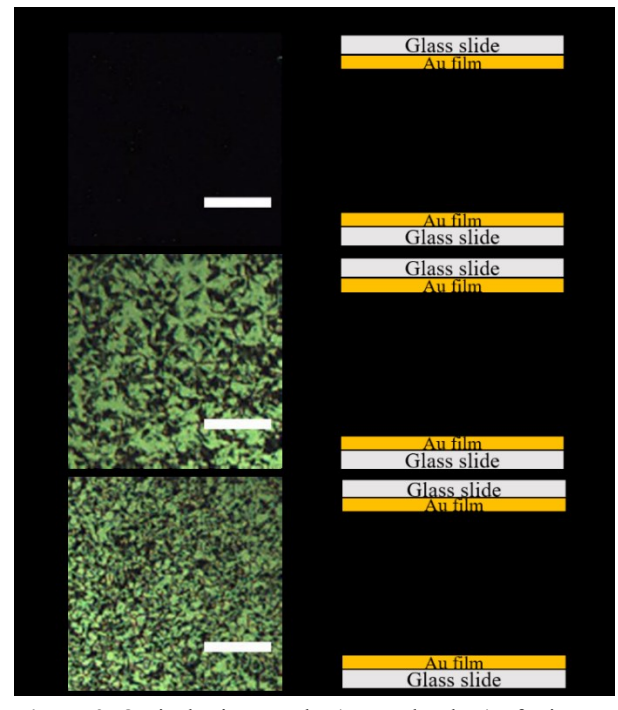


**Figure 2.** Optical micrographs (crossed polars) of micrometer-thick films of (a) CBCA-5CB ( $C_{\rm CBCA} = 0.1 \, {\rm mol\%}$ ) (b) CBCM-5CB ( $C_{\rm CBCM} = 0.1 \, {\rm mol\%}$ ) or (c) CBCNa-5CB ( $C_{\rm CBCNa} = 0.1 \, {\rm mol\%}$ ) sandwiched between two gold films. Scale bar: 200 µm. A schematic representation of the LCs is shown to the side of each optical image and black lines indicate the director of LCs.

To provide insight into the molecular interactions of CBCA, CBCM and CBCNa with the Au films, we used IR spectroscopy<sup>75</sup> (a summary of the peak assignments is listed in Table 2).

Prior to performing PM-IRRAS, we measured the mid-wavenumber spectra of bulk samples of the three compounds by transmission FTIR spectroscopy. These measurements confirmed that the positions of the nitrile peaks for all three molecules lie between 2248-2225 cm<sup>-1</sup> (Figure 3a). To perform the PM-IRRAS measurements, we spin-coated thin films (ellipsometric thicknesses of ~2 nm) of either CBCA, CBCM or CBCNa onto the gold films. Inspection of the IR spectra shown in Figure 3b reveals that the peak corresponding to the nitrile group is evident for CBCA but not CBCM or CBCNa. This observation, when combined with the surface-selection rules for IR spectroscopy on gold films<sup>76</sup>, indicates that the nitrile group of CBCA has a transition dipole moment that projects onto the normal of the gold surface. In contrast, the absence of the nitrile peak for both CBCM and CBCNa indicate that these two compounds adsorbed in an orientation that places the transition dipole moment of the nitrile group parallel to the gold surface. These molecular orientations determined by PM-IRRAS are consistent with the macroscopic orientations of the LC phases containing CBCA, CBCM and CBCNa (Figure 2a-c).

**Table 2.** Vibrational frequency (cm<sup>-1</sup>) assignments for peaks in Figure 3.  $\nu$  represents stretching and  $\beta$  represents in-plane bending.

Assignment	Measured Frequency <sup>77,78</sup>	Calculated Frequency
v(C≡N)	2248-2225	2271
ν(C=O)	1695, 1681	1685
$\nu(C\text{-}C)_{ring}$	1609, 1604	1602
$\nu(C\text{-}C)_{ring}$	1429, 1425	1437
β(О–Н)	1400	1385

To provide additional insight into the interaction of CBCA with the gold surface that gives rise to the perpendicular orientation, we examined IR modes associated with the carboxylic acid of bulk CBCA (Figure 3c) and a thin film of CBCA (Figure 3d, I) deposited onto a gold film. Past studies have reported that aromatic carboxylic acids can form carboxylate anions on gold surfaces<sup>35,36,79</sup>. We considered the possibility that CBCA binds to the surfaces of the gold films used in our experiments via formation of a carboxylate anion. However, inspection of Figure 3d, I reveals the absence of a peak at 1380 cm<sup>-1</sup> characteristic of a carboxylate anion. Our conclusion that the carboxylate anion is not formed on the gold surfaces used in our study is supported by past reports that carboxylate anions only form on gold surfaces in the presence of an externally applied oxidizing potential. <sup>79 35,36</sup>.

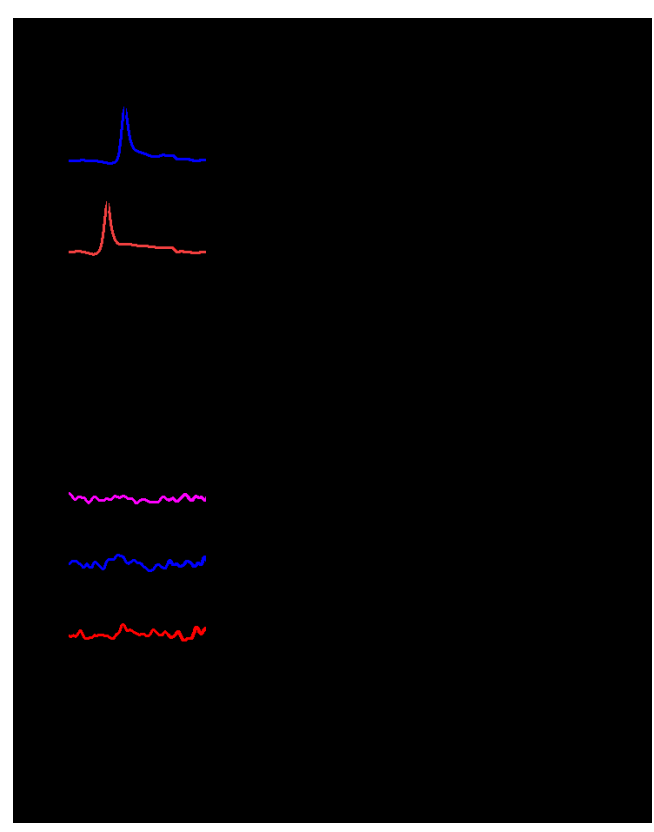


**Figure 3.** (a) Transmission IR spectra of solid (I) CBCA (II) CBCNa and (III) CBCM in the nitrile stretch region. (b) PM-IRRAS of nanometer-thick layers of (I) CBCA (II) CBCNa or (III) CBCM on gold films (IV) CBCA on gold films exposure to Cl<sub>2</sub> gas. (c) Transmission IR spectrum of solid CBCA showing OH in-plane bending modes and C-C stretching vibrations (d) PM-IRRAS of nanometer-thick layers of CBCA deposited onto (I) a gold film (II) a gold film exposure to Cl<sub>2</sub>.

We also considered the possibility that defects and adatoms on the gold surfaces used in our study may cause binding of CBCA as carboxylic acids, as has been proposed computationally<sup>80</sup>. However, inspection of Fig. 4d, I reveals the absence of the O-H in-plane bending mode at 1400 cm<sup>-1</sup> in the IR spectra of bound CBCA (see Figure S8 for additional experimental results supporting this conclusion). The absence of the O-H bending mode is, however, consistent with CBCA bound on the surface as a dehydrogenated species. To explore this hypothesis, we calculated the minimum energy path for the adsorption and dehydrogenation of PhCOOH on Au(111) (Figure 4a). We found that the dehydrogenation step is characterized by an activation energy barrier of 1.61 eV with respect to the most stable (parallel) adsorbed PhCOOH state (Figure 1 and Table 1). This barrier height will prevent PhCOOH dehydrogenation at room temperature. Furthermore, the dehydrogenation step is energetically uphill by 1.31 eV on Au(111), which is in agreement with previous experimental findings<sup>81</sup>. Past studies, however, have revealed that adsorbed species, such as oxygen, facilitate dehydrogenation in our experiments<sup>39</sup>. Thus, it appears likely that adsorbates such as O or adventitious carbon present on the gold films (see Figure S9 for XPS evidence) facilitate CBCA dehydrogenation evident in our IR measurement. It is also possible

that step-edges, kinks, and other defect sites present on the polycrystalline Au surfaces used in our experiments facilitate CBCA dehydrogenation. Finally, we note that the appearance of peaks at 1609 and 1429 cm<sup>-1</sup> in Figure 3d, I, which correspond to the C-C stretching vibrations of an aromatic ring, indicate a dipole moment that projects onto the normal of the gold surface. This result further reinforces our conclusion that CBCA binds to the gold surface in a perpendicular orientation (and that the OH group, if present when CBCA is bound to the gold surface, would be observed in the IR spectra).

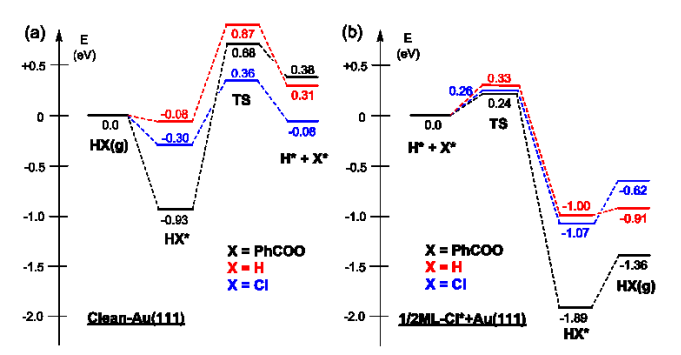


**Figure 4.** Calculated potential energy diagram for (a) adsorption and dissociation of H<sub>2</sub>, HCl, and PhCOOH on clean Au(111) ((4x4) unit cell) and (b) recombinative desorption of H<sub>2</sub>, HCl, and PhCOOH on 0.5 ML Cl-covered Au(111) ((4x4) unit cell). '\* and '+' indicate surface adsorbed species and infinitely separated states, respectively. 'TS' refers to transition state. All energies are in eV. For PhCOOH\* and PhCOO\*, the most stable parallel and perpendicular orientation is considered, respectively (see details in Table 1).

Motivated by our hypothesis that CBCA is bound to the gold surfaces used in our study as a dehydrogenated species, we studied the fate of the H atoms generated from CBCA dehydrogenation (Figure 4a). On Au(111), H recombinative desorption to  $H_2(g)$  is energetically favorable by -0.31 eV, with a desorption energy barrier of 0.56 eV, which can be overcome close to room temperature. Similarly, the energetics shown in Figure 4a suggest that adsorbed H atoms may alternatively react with adsorbed Cl atoms (see below for studies of  $Cl_2$ ) to evolve HCl(g).

Computational predictions and experimental characterization of the influence of Cl adatoms on the orientations of LCs on Au(111). Next we studied Cl<sub>2</sub> adsorption on PhCOO-covered Au(111) surfaces. Through our computations, we predicted that chlorine will spontaneously dissociatively adsorb even in the presence of 3 PhCOO adsorbates in a (3x3) unit cell, which is the saturation coverage for PhCOO in a (3x3) unit cell. This result suggests that Cl should adsorb even in the presence of LC on Au(111). To understand the effect of adsorbed Cl on the surface-bound LC layer under experimental conditions, we developed a phase diagram to predict Cl coverage on Au(111) over a wide temperature and Cl<sub>2</sub> pressure (Cl chemical potential) range (Figure 5a, see details in Methods section). Under experimentally relevant conditions, ambient temperature and 1 ppm Cl<sub>2</sub>, we predict 0.5 ML Cl coverage on Au(111) at equilibrium (Figure 5a white area). Based on this prediction, we studied the binding of CBCA surrogates on 0.5 ML Cl pre-covered

Au(111) in a (4x4) unit cell. We found that the BE of PhCOO in the perpendicular orientation is only -1.82 eV relative to PhCOO(g) while we note that the BE of PhCOO in perpendicular orientation on clean Au(111) is -2.50 eV. This difference in BE (0.68 eV) indicates a strong destabilization of PhCOO due to the presence of Cl on Au(111), which may translate into its displacement from Au, upon exposure to Cl<sub>2</sub>(g). Figure 4b provides the calculated energetics of three competing elementary processes for elimination of adsorbed H from Au(111) covered with 1/2ML of Cl\* (spectator species). Adsorbed H is a product of CBCA dehydrogenation on Au(111) prior to exposure to Cl<sub>2</sub>(g). Under these conditions, all three elementary processes described earlier (see discussion of Figure 4a) are kinetically easier than they are on the clean Au(111) surface. In fact, the three transition state energies are very close to each other, suggesting that H atoms from CBCA dehydrogenation, in the presence of adsorbed Cl atoms, can either desorb as H<sub>2</sub> or HCl or reform CBCA. Overall, we predict that the binding of PhCOO is not favored on 0.5 ML Cl covered Au(111), and that increasing Cl coverage will decrease coverage of the CBCAderived carboxyl and trigger an orientational transition of CBCA-doped 5CB.

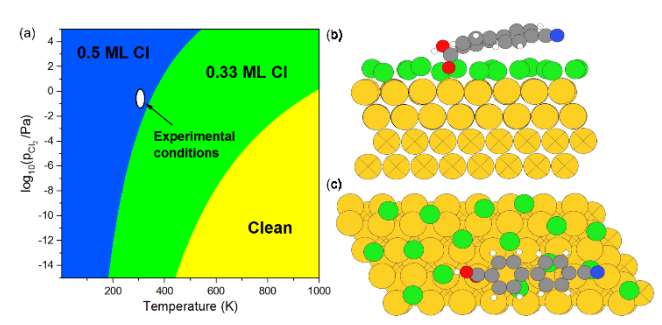


**Figure 5.** (a) Calculated phase diagram of Cl coverage on Au(111) as a function of Cl<sub>2</sub>(g) pressure (chemical potential) and temperature. (b) Side view and (c) top view of the calculated minimum energy structure of CBCA on 0.5 ML Cl precovered Au(111) surface in a (8x4) unit cell. White, grey, green, red, yellow, and blue colors indicate H, C, Cl, O, Au and N atoms, respectively. Crossed atoms were not allowed to relax during energy minimization.

To assess the above-described computational predictions via experiment, CBCA-5CB mixtures with a range of CBCA concentrations (0.005 mol%, 0.002 mol% and 0.001 mol%) were deposited onto gold films and subsequently exposed to gaseous Cl<sub>2</sub>. As shown in Figure S10, prior to exposure to Cl<sub>2</sub>, the CBCA-5CB mixture containing the lowest concentration of CBCA (0.001 mol%) did not exhibit a homeotropic orientation, while the two mixtures with CBCA concentrations of 0.002 mol% and 0.005 mol% induced homeotropic orientations. Because the BE of CBCA to Au(111) surfaces is highly favorable relative to 5CB (Table 1) and the equilibrium constant of the binding exchange process is calculated to be  $K = 1.1 \times 10^4$ , we predicted that almost all CBCA in the 5CB mixture will bind to the Au(111) surface (see SI for details). For the mixture containing (see details in SI) 0.001 mol\% CBCA in 5CB, we calculated that CBCA-derived carboxylates form only 0.035 ML

on the gold surface, a concentration that our experimental results indicate is insufficient to cause a homeotropic orientation of the LC

We exposed the Au(111)-supported LC mixtures containing 0.002 mol% CBCA in 5CB to a nitrogen stream containing 1 ppm Cl<sub>2</sub>. As shown in Figure 6, the CBCA-5CB mixtures transitioned away from the initial homeotropic orientation upon exposure to Cl<sub>2</sub>. The change in optical interference colors generated using white-light illumination was consistent with the LC assuming a planar orientation on the gold surface decorated with Cl adatoms (see Figure 6b). Subsequent exposure of the samples to N<sub>2</sub> for 1 hour did not result in a change in orientation of the LC. The irreversible optical response of the LC to Cl adsorption supports our conclusion of strong binding of Cl to Au (111). 33,82

As shown in Figure 7a, the mixture of 5CB and 0.002 mol% CBCA exhibited an anchoring transition with dynamics that were faster than 5CB mixed with 0.005 mol% CBCA, presumably because Cl<sub>2</sub> has to displace more CBCA from the Au(111) surface in the 0.005 mol% CBCA sample than that for the 0.002 mol% CBCA sample to trigger the anchoring transition of the LC. To verify the hypothesis of CBCA-coverage dependent response time, we investigated CBCA-5CB compositions with increasing CBCA content up to the concentration at which CBCA-derived carboxyl species reached saturation coverage on the Au surface, after which point the response time should not change with increasing CBCA concentration. Our computational analysis suggested that CBCA-derived carboxyl species reached a saturation coverage of 1/3 ML at Au(111) in a (3x3) unit cell that is equivalent to 0.01 mol% CBCA concentration (details of calculations can be found in the SI). Figure 7a shows that 0.01 mol% CBCA in 5CB clearly exhibited a slower anchoring transition than that of 0.005 mol% CBCA in 5CB while there was no significant change in response time between samples containing 0.01 and 0.1 mol% CBCA in 5CB. Thus, these anchoring transition experiments provide additional support for our computational models and our understanding of atomicscale interfacial processes occurring at Au-LC interfaces.

We performed several control experiments to confirm that the optical response of the LC shown in Figure 6 was triggered by dissociative adsorption of Cl<sub>2</sub> on the surface of the gold film. Because Cl<sub>2</sub> is a strong oxidizing agent, we consider it possible that oxidation of 5CB may play a role in the optical response shown in Figure 6b. As shown in Table S1, however, we measured the nematic-to-isotropic transition temperature (T<sub>NI</sub>) of the CBCA-5CB mixture to not measurably change upon exposure to 1 ppm Cl<sub>2</sub> for one hour, a timescale that is well beyond the chemoresponse reported in Figure 7a. Two additional control experiments were performed to minimize the possibility that the response in Figure 6b was due to a reaction between Cl<sub>2</sub> and the bulk CBCA-5CB mixture ( $C_{CBCA} = 0.002 \text{ mol}\%$ ): (i) we exposed the CBCA-5CB mixture to Cl<sub>2</sub> gas, subsequently placed the LC on a gold film and observed a homeotropic orientation (Figure S11a) and (ii) a gold film was exposed to Cl<sub>2</sub> and then contacted with the CBCA-5CB mixture; the substrate caused a planar orientation of the LC mixture (Figure S11b). Finally, we performed XPS measurements of Au films before and after exposure to Cl<sub>2</sub>. The Au films were coated with micrometer-thick films of LC, exposed to Cl2, and then rinsed with ethanol to remove the LC prior to performing XPS. After exposure, a peak corresponding to Cl 2p at 197.7 eV is clearly evident (Figure 7b, I). In contrast, no equivalent peak was evident on the Au surface prior to exposure to the Cl<sub>2</sub> gas (Figure 7b, II).

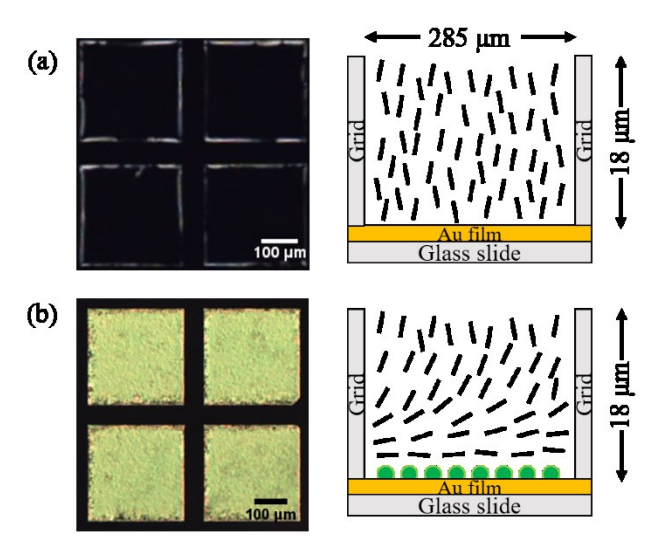


**Figure 6.** Optical micrographs (crossed polars) of micrometer-thick films of CBCA-5CB mixture ( $C_{\rm CBCA} = 0.002$  mol%) supported on gold surfaces (a) initial state (b) exposed to a vapor of 1 ppm Cl<sub>2</sub> for 15 mins. A schematic representation of the LCs is shown to the side of each optical image. Black lines indicate the director of LCs. Green circles indicate the adsorbed Cl atoms. Scale bar: 100 μm.

Additional insight into the influence of the adlayer of Cl on the molecular interactions between CBCA and gold were obtained by using PM-IRRAS. As shown in Figure 3b, IV and 4d, II, the IR band corresponding to the nitrile peak and C-C stretching peak, both of which are evident prior to the exposure to Cl<sub>2</sub>, are not present when CBCA contacts the Cl<sub>2</sub>-treated Au surface. This result is consistent with the planar orientation of the CBCA-5CB film on the gold surface after exposure to Cl<sub>2</sub>. In addition, as shown in Figure 3d, II, we measured exposure of the Au films to Cl2 gas to lead to the reappearance of the O-H in-plane bending peak at 1400 cm<sup>-1</sup>, providing evidence that the Cl adlayer prevents dehydrogenation of the CBCA (thus leading to planar anchoring). Interesting, we observed IR peaks associated with the carbonyl and hydroxyl groups, but not the phenyl groups. To provide insight into this observation, we calculated the binding of a CBCA molecule on 0.5 ML Cl covered Au(111). We found a state, which is more stable than physisorbed CBCA by 0.12 eV, achieved by rotating the carboxylic group plane relative to the phenyl ring of CBCA. In this adsorbed state (Figure 5b), the carbonyl group can directly interact with the Au surface. The hydroxyl group points toward a Cl adatom forming a hydrogen bond, and the phenyl rings and the nitrile group of CBCA adopt a parallel orientation on the surface. This state is consistent with the above-described peaks of the IR spectrum of CBCA molecules on Cl-covered Au surfaces. Overall, these experiments provide additional support for our conclusion that the orientational response seen in Figure 6b is due to dissociative adsorption of Cl<sub>2</sub> on the surface of the supporting Au films.

Sensitivity and selectivity. Cl<sub>2</sub> gas is a toxic and potential work-place hazard, and deliberate exposure has been used both historically and recently as a tool of chemical warfare. 81-83 To determine the relevance of the findings reported in this paper as the basis of future wearable measurement tools to protect against human exposure to Cl<sub>2</sub> gas, we determined the time taken for the CBCA-5CB mixture to respond to human exposure limits specified by the US occupational Safety and Health Administration (OSHA). OSHA specifies short-term exposure limit for humans to be 15 minutes at 1ppm Cl<sub>2</sub>.86 We defined the response time of the LC as the time to reach 20% of the full optical response of the LC. Inspection of Figure 7a and 8 reveals that the response time of the CBCA-5CB mixture ( $C_{CBCA}$  = 0.002 mol%) to 1 ppm Cl<sub>2</sub> was 5 mins, well within the 15 mins exposure limit. OSHA also specifies an 8-hour exposure limit (time-weighted average) as 500 ppb Cl<sub>2</sub>. Accordingly, we characterized the dynamic response of CBCA-5CB mixtures (C<sub>CBCA</sub> = 0.002 mol%) supported on the Au films following exposure

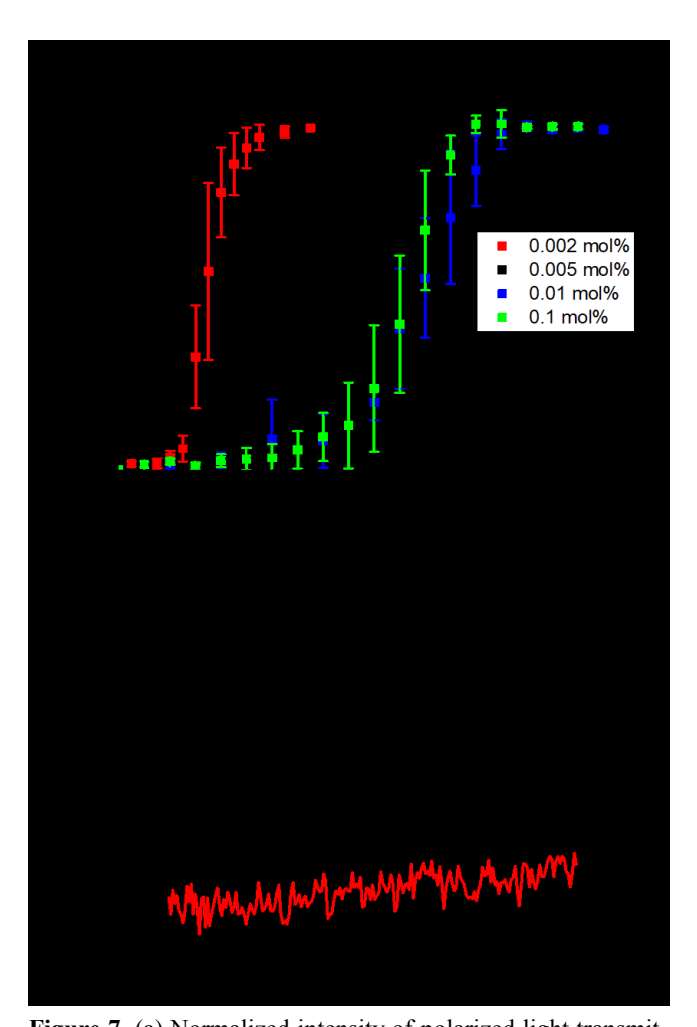


**Figure 7.** (a) Normalized intensity of polarized light transmitted through LCs supported on gold surfaces and then exposed to a vapor of 1 ppm  $Cl_2$  for  $C_{CBCA} = 0.002$ , 0.005, 0.01 and 0.1 mol%, with 5 replicates respectively. (b) XPS showing (I) Cl 2p peaks at 197.7 eV and 199.3 eV on Au surface following exposure to  $Cl_2$  gas and (II) Au film prior to exposure to  $Cl_2$  gas.

to 200 ppb or 500 ppb Cl<sub>2</sub>. Inspection of Figure 8 reveals that the LC mixture responds to 500 ppb Cl<sub>2</sub> within 9 mins and to 200 ppb Cl<sub>2</sub> within 19 mins, establishing the relevancy of our results to long-term human exposure monitoring to Cl<sub>2</sub> gas.

We also investigated the selectivity of our LC-based system to  $\text{Cl}_2$  relative to other chemical species such as gaseous  $\text{N}_2$ , dimethyl methylphosphonate (DMMP), ammonia, ethylene oxide, and formaldehyde. Our computational results predicted weak binding of all of these compounds to Au(111) surfaces relative to CBCA (Table S2) and, therefore, that the 5CB-CBCA mixture should not respond to these potentially interfering compounds. Consistent with this prediction, following exposure of the CBCA-5CB mixture ( $C_{\text{CBCA}} = 0.002 \text{ mol}\%$ ) to 80 % relative humidity in  $\text{N}_2$  and 5 ppm (in  $\text{N}_2$ ) DMMP, ammonia, ethylene oxide, and formaldehyde for 1 hour, we did not observe any change in the orientation of the LC (Figure S12). This result supports a selectivity based on dissociative adsorption of  $\text{Cl}_2$  on the Au surface in the presence of CBCA. (Additional discussion can be found in SI)

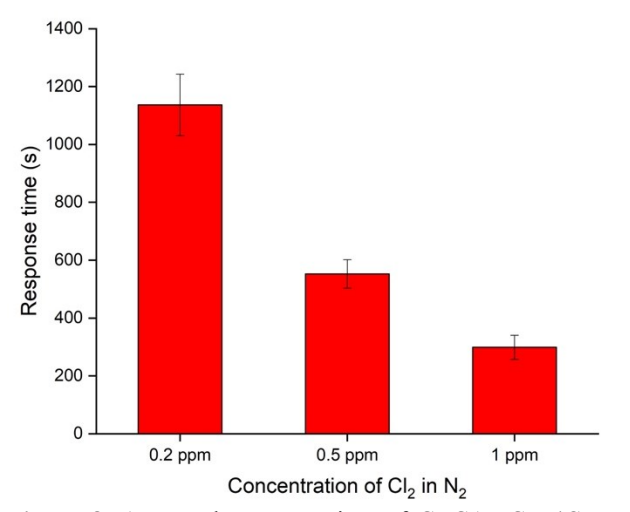


**Figure 8.** Averaged response time of CBCA-5CB ( $C_{\rm CBCA} = 0.002 \, \text{mol}\%$ ) mixtures on gold films to 0.2 ppm, 0.5 ppm and 1 ppm Cl<sub>2</sub> in N<sub>2</sub> from 5 replicates respectively. The response time is defined as the time required to reach 20% normalized light intensity of full response.

#### CONCLUSIONS

The key result reported in this paper is the design of a LC system that amplifies atomic-scale processes involving dissociative adsorption of Cl<sub>2</sub> and dehydrogenation of carboxylic acid groups on gold surfaces *in situ* into macroscopic optical signals. The results are conceptually important because they demonstrate that it is possible to leverage past studies of elementary reaction steps on transition metal surfaces performed in the context of surface science and heterogeneous catalysis to design surfaces that orient LCs and trigger orientational transitions in LCs in response to targeted atomic-scale transformations on surfaces. <sup>87–89</sup> Specifically, we used a combination of computational chemistry methods and experiments to show that aromatic molecules with carboxylic acid groups exhibit strong directional binding to gold surfaces as a consequence of dehydrogenation of the carboxylic group. Dissociative adsorption of Cl<sub>2</sub>

gas on the Au surface weakens binding of the dehydrogenated carboxylic acid, thus triggering an orientational change in LCs doped with the aromatic carboxylic acids. Our results also generate a range of fundamental questions: (i) what is the role of surface defects and their density on the Au surface on the response of LCs? (ii) what determines the minimum surface coverage of CBCA needed to achieve homeotropic ordering in the mixture with 5CB? and (iii) what molecular processes on the surface are dictating the dynamics of the response of the LC to chlorine gas? We envisage a range of future directions of investigation to address these and other questions. For example, alloys of noble and Pt-group metals have been shown to provide rich opportunities to tune atomic-scale interactions with adsorbates, with profound consequences for their catalytic properties. 90,91 Such atomically tailored surfaces appear promising as tunable substrates for designing LC systems that respond to elementary surface reaction steps other than dissociative adsorption and dehydrogenation. In an applied context, we also note that a key practical advantage of the approach described in this paper for design of chemoresponsive LCs is the stability of the Au(111)-LC interface relative to metal salt-decorated surfaces that have been shown previously to permit reporting of binding and redox processes using LCs. <sup>48,59,92,93</sup> More broadly, the study in this paper advances our understanding of the interactions of structured liquids with metal surfaces.<sup>21</sup> Additionally, understanding the behaviors of organic molecules, such as nitrile- or carboxylic acid-containing molecules, at metal surfaces is relevant to a range of emerging technologies, including flow chemistry<sup>94,95</sup> or nanofluidics<sup>96,97</sup>.

#### AUTHOR INFORMATION

Corresponding Author

\*emavrikakis@wisc.edu (Manos Mavrikakis)

\*nabbott@cornell.edu (Nicholas L. Abbott)

**Author Contributions** 

<sup>+</sup>H.Y. and T.S. contributed equally to this work.

Notes

N.L.A. declares a financial interest in Platypus Technologies LLC, a for-profit company that has developed LC-based analytic technologies. A US patent application has been filed by University of Wisconsin-Madison based on the results described in this paper.

#### ACKNOWLEDGMENT

This work was supported by the National Science Foundation (DMREF grant DMR-1435195 and DMR-1921722) and the Army Research Office (W911NF-14-1-0140). Part of the computational work conducted by T.S. and M.M. in this study was carried out through external computational resource facilities at: the DoD High Performance Computing Modernization Program (US Air Force Research Laboratory DoD Supercomputing Resource Center (AFRL DSRC), the US Army Engineer Research and Development Center (ERDC), and the Navy DoD Supercomputing Resource Center (Navy DSRC), ARONC43623362), supported by the Department of Defense; the National Energy Research Scientific Computing Center

(NERSC) through the U.S. DOE, Office of Science under Contract No. DE-AC02-05CH11231; and the Center for Nanoscale Materials (CNM) at Argonne National Laboratory (ANL) through the U.S. DOE, Office of Science under Contract No. DE-AC02-06CH11357.

#### REFERENCES

- (1) Sadati, M.; Ramezani-Dakhel, H.; Bu, W.; Sevgen, E.; Liang, Z.; Erol, C.; Rahimi, M.; Taheri Qazvini, N.; Lin, B.; Abbott, N. L.; Molecular Structure of Canonical Liquid Crystal Interfaces. *J. Am. Chem. Soc.* 2017, 139 (10), 3841–3850.
- (2) Claridge, S. A.; Liao, W. S.; Thomas, J. C.; Zhao, Y.; Cao, H. H.; Cheunkar, S.; Serino, A. C.; Andrews, A. M.; Weiss, P. S. From the Bottom up: Dimensional Control and Characterization in Molecular Monolayers. *Chem. Soc. Rev.* 2013, 42 (7), 2725– 2745
- Wang, M.; Nudelman, F.; Matthes, R. R.; Shaver, M. P. Frustrated Lewis Pair Polymers as Responsive Self-Healing Gels. J. Am. Chem. Soc. 2017, 139 (40), 14232–14236.
- (4) Campbell, M. G.; Liu, S. F.; Swager, T. M.; Dinca, M. Chemiresistive Sensor Arrays from Conductive 2D Metal-Organic Frameworks. J. Am. Chem. Soc. 2015, 137 (43), 13780– 13783.
- (5) Mavila, S.; Worrell, B. T.; Culver, H. R.; Goldman, T. M.; Wang, C.; Lim, C. H.; Domaille, D. W.; Pattanayak, S.; McBride, M. K.; Musgrave, C. B.; Dynamic and Responsive DNA-like Polymers. J. Am. Chem. Soc. 2018, 140 (42), 13594–13598.
- (6) Han, Y.; Pacheco, K.; Bastiaansen, C. W. M.; Broer, D. J.; Sijbesma, R. P. Optical Monitoring of Gases with Cholesteric Liquid Crystals. J. Am. Chem. Soc. 2010, 132 (9), 2961–2967.
- (7) Schwartz, J. J.; Mendoza, A. M.; Wattanatorn, N.; Zhao, Y.; Nguyen, V. T.; Spokoyny, A. M.; Mirkin, C. A.; Baše, T.; Weiss, P. S. Surface Dipole Control of Liquid Crystal Alignment. *J. Am. Chem. Soc.* 2016, *138* (18), 5957–5967.
- (8) Su, X.; Voskian, S.; Hughes, R. P.; Aprahamian, I. Manipulating Liquid-Crystal Properties Using a pH Activated Hydrazone Switch. Angew. Chemie - Int. Ed. 2013, 52 (41), 10734–10739.
- (9) Manna, U.; Zayas-Gonzalez, Y. M.; Carlton, R. J.; Caruso, F.; Abbott, N. L.; Lynn, D. M. Liquid Crystal Chemical Sensors That Cells Can Wear. *Angew. Chemie - Int. Ed.* 2013, 52 (52), 14011– 14015.
- (10) Shah, R. R.; Abbott, N. L. Principles for Measurement of Chemical Exposure Based on Recognition-Driven Anchoring Transitions in Liquid Crystals. Science 2001, 293 (5533), 1296– 1299
- (11) Nayani, K.; Kim, Y.-K.; Abbott, N. L. Chiral Interactions in Liquid Crystals. *Nat. Mater.* **2018**, *17* (1), 14–15.
- (12) Yuan, Y.; Martinez, A.; Senyuk, B.; Tasinkevych, M.; Smalyukh, I. I. Chiral Liquid Crystal Colloids. *Nat. Mater.* 2018, 17, 71–78.
- (13) Brake, J. M.; Daschner, M. K.; Luk, Y.; Abbott, N. L. Biomolecular Interactions at Phospholipid-Decorated Surfaces of Liquid Crystal. Science 2010, 302 (5653), 2094–2097.
- (14) Lockwood, N.; Gupta, J.; Abbott, N. Self-Assembly of Amphiphiles, Polymers and Proteins at Interfaces between Thermotropic Liquid Crystals and Aqueous Phases. Surf. Sci. Rep. 2008, 63 (6), 255–293.
- (15) Carlton, R. J.; Hunter, J. T.; Miller, D. S.; Abbasi, R.; Mushenheim, P. C.; Tan, L. N.; Abbott, N. L. Chemical and Biological Sensing Using Liquid Crystals. *Liq. Cryst. Rev.* **2013**, *1* (1), 29–51.
- (16) Lin, I.-H.; Miller, D. S.; Bertics, P. J.; Murphy, C. J.; de Pablo, J. J.; Abbott, N. L. Endotoxin-Induced Structural Transformations in Liquid Crystalline Droplets. *Science* 2011, 332 (6035), 1297–1300.
- (17) Wang, X.; Miller, D. S.; Bukusoglu, E.; de Pablo, J. J.; Abbott, N. L. Topological Defects in Liquid Crystals as Templates for Molecular Self-Assembly. *Nat. Mater.* 2016, 15 (1), 106–112.
- (18) Wang, X.; Kim, Y. K.; Bukusoglu, E.; Zhang, B.; Miller, D. S.; Abbott, N. L. Experimental Insights into the Nanostructure of the Cores of Topological Defects in Liquid Crystals. *Phys. Rev. Lett.* 2016, 116 (14), 1–5.

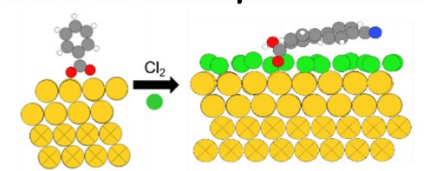
- (19) Kim, D. W.; Ok, J. M.; Jung, W. Bin; Kim, J. S.; Kim, S. J.; Choi, H. O.; Kim, Y. H.; Jung, H. T. Direct Observation of Molybdenum Disulfide, MoS2, Domains by Using a Liquid Crystalline Texture Method. *Nano Lett.* 2015, 15 (1), 229–234.
- (20) Smith, D. P. E.; Horber, H.; Gerber, C.; Binning, G. Smectic Liquid Crystal Monolayers on Graphite Observed by Scanning Tunneling Microscopy. *Science* 1989, 245 (4913), 43–45.
- (21) Sanda, P. N.; Dove, D. B.; Ong, H. L.; Jansen, S. A.; Hoffmann, R. Role of Surface Bonding on Liquid-Crystal Alignment at Metal Surfaces. *Phys. Rev. A* 1989, 39 (5), 2653–2658.
- (22) Culp, J. T.; Park, J. H.; Stratakis, D.; Meisel, M. W.; Talham, D. R. Supramolecular Assembly at Interfaces: Formation of an Extended Two-Dimensional Coordinate Covalent Square Grid Network at the Air-Water Interface. J. Am. Chem. Soc. 2002, 124 (34), 10083–10090.
- (23) Kampschulte, L.; Heckl, W. M.; Lackinger, M.; Werblowsky, T. L.; Kishore, R. S. K.; Schmittel, M. Thermodynamical Equilibrium of Binary Supramolecular Networks at the Liquid-Solid Interface. J. Am. Chem. Soc. 2008, 130 (26), 8502–8507.
- (24) Mann, S.; Ozin, G. A. Synthesis of Inorganic Materials with Complex Form. *Nature* **1996**, *382* (6589), 313–318.
- (25) Grosso, D.; Ribot, F.; Boissiere, C.; Sanchez, C. Molecular and Supramolecular Dynamics of Hybrid Organic-Inorganic Interfaces for the Rational Construction of Advanced Hybrid Nanomaterials. *Chem. Soc. Rev.* 2011, 40 (2), 829–848.
- (26) Binder, W. H. Supramolecular Assembly of Nanoparticles at Liquid-Liquid Interfaces. Angew. Chemie - Int. Ed. 2005, 44 (33), 5172–5175.
- (27) Dongping, Z.; Velmurugan, J.; Mirkin, M. V. Adsorption/Desorption of Hydrogen on Pt Nanoelectrodes: Evidence of Surface Diffusion and Spillover. J. Am. Chem. Soc. 2009, 131 (41), 14756–14760.
- (28) Zhang, C. J.; Hu, P. CO Oxidation on Pd(100) and Pd(111): A Comparative Study of Reaction Pathways and Reactivity at Low and Medium Coverages. J. Am. Chem. Soc. 2001, 123 (6), 1166– 1172
- (29) Montemore, M. M.; Medlin, J. W. A Unified Picture of Adsorption on Transition Metals through Different Atoms. J. Am. Chem. Soc. 2014, 136 (26), 9272–9275.
- (30) Zhang, J.; Vukmirovic, M. B.; Xu, Y.; Mavrikakis, M.; Adzic, R. R. Controlling the Catalytic Activity of Platinum-Monolayer Electrocatalysts for Oxygen Reduction with Different Substrates. Angew. Chemie - Int. Ed. 2005, 44 (14), 2132–2135.
- (31) Alayoglu, S.; Nilekar, A. U.; Mavrikakis, M.; Eichhorn, B. Ru-Pt Core-Shell Nanoparticles for Preferential Oxidation of Carbon Monoxide in Hydrogen. *Nat. Mater.* 2008, 7 (4), 333–338.
- (32) Nilekar, A. U.; Sasaki, K.; Farberow, C. A.; Adzic, R. R.; Mavrikakis, M. Mixed-Metal Pt Monolayer Electrocatalysts with Improved CO Tolerance. J. Am. Chem. Soc. 2011, 133 (46), 18574–18576.
- (33) Kastanas, G. N.; Koel, B. E. Interaction of Cl2 with the Au(111) Surface in the Temperature Range of 120 to 1000 K. Appl. Surf. Sci. 1993, 64 (3), 235–249.
- (34) Gao, W.; Baker, T. A.; Zhou, L.; Pinnaduwage, D. S.; Kaxiras, E.; Friend, C. M. Chlorine Adsorption on Au(111): Chlorine Overlayer or Surface Chloride? J. Am. Chem. Soc. 2008, 130 (11), 3560–3565.
- (35) Han, B.; Li, Z.; Wandlowski, T. Adsorption and Self-Assembly of Aromatic Carboxylic Acids on Au/Electrolyte Interfaces. *Anal. Bioanal. Chem.* 2007, 388 (1), 121–129.
- (36) Li, H. Q.; Roscoe, S. G.; Lipkowski, J. FTIR Studies of Benzoate Adsorption on the Au(111) Electrode. *J. Electroanal. Chem.* 1999, 478 (1–2), 67–75.
- (37) McEntee, M.; Tang, W.; Neurock, M.; Yates, J. T. Mechanistic Insights into the Catalytic Oxidation of Carboxylic Acids on Au/TiO2: Partial Oxidation of Propionic and Butyric Acid to Gold Ketenylidene through Unsaturated Acids. ACS Catal. 2015, 5 (2), 744–753.
- (38) McEntee, M.; Tang, W.; Neurock, M.; Yates, J. T. Selective Catalytic Oxidative-Dehydrogenation of Carboxylic Acids—Acrylate and Crotonate Formation at the Au/TiO2 Interface. *J. Am. Chem. Soc.* **2014**, *136* (13), 5116–5120.
- (39) Schwarz, D.; Van Gastel, R.; Zandvliet, H. J. W.; Poelsema, B.

- In Situ Observation of a Deprotonation-Driven Phase Transformation: 4,4'-Biphenyldicarboxylic Acid on Au(111). *J. Phys. Chem. C* **2013**, *117* (2), 1020–1029.
- (40) Cebula, I.; Smith, E. F.; Gimenez-Lopez, M. D. C.; Yang, S.; Schröder, M.; Champness, N. R.; Beton, P. H. Packing of Isophthalate Tetracarboxylic Acids on Au(111): Rows and Disordered Herringbone Structures. J. Phys. Chem. C 2013, 117 (36), 18381–18385.
- (41) Siler, C. G. F.; Cremer, T.; Rodriguez-Reyes, J. C. F.; Friend, C. M.; Madix, R. J. Switching Selectivity in Oxidation Reactions on Gold: The Mechanism of C–C vs C–H Bond Activation in the Acetate Intermediate on Au(111). ACS Catal. 2014, 4 (9), 3281–3288
- (42) Gazsi, A.; Bánsági, T.; Solymosi, F. Decomposition and Reforming of Formic Acid on Supported Au Catalysts: Production of CO-Free H2. J. Phys. Chem. C 2011, 115 (31), 15459–15466.
- (43) Singh, S.; Li, S.; Carrasquillo-Flores, R.; Alba-Rubio, A. C.; Dumesic, J. A.; Mavrikakis, M. Formic Acid Decomposition on Au Catalysts: DFT, Microkinetic Modeling, and Reaction Kinetics Experiments. *AIChE J.* **2014**, *60* (4), 1303–1319.
- (44) Herron, J. A.; Scaranto, J.; Ferrin, P.; Li, S.; Mavrikakis, M. Trends in Formic Acid Decomposition on Model Transition Metal Surfaces: A Density Functional Theory Study. ACS Catal. 2014, 4 (12), 4434–4445.
- (45) Steiner, U. B.; Caseri, W. R.; Suter, U. W. Adsorption of Alkanenitriles and Alkanedinitriles on Gold and Copper. *Langmuir* **1992**, *8* (11), 2771–2777.
- (46) Chen, A.; Yang, D.; Lipkowski, J. Electrochemical and FTIR Studies of 4-Cyanopyridine Adsorption at the Gold(111)|solution Interface. J. Electroanal. Chem. 1999, 475 (2), 130–138.
- (47) Pluchery, O.; Tadjeddine, M.; Flament, J.; Tadjeddine, A. Adsorption of 4-Cyanopyridine on Au(111): Ab Initio Calculations and SFG Measurements. *Phys. Chem. Chem. Phys.* **2001**, *3* (16), 3343–3350.
- (48) Szilvási, T.; Bao, N.; Nayani, K.; Yu, H.; Rai, P.; Twieg, R. J.; Mavrikakis, M.; Abbott, N. L. Redox-Triggered Orientational Responses of Liquid Crystals to Chlorine Gas. *Angew. Chemie - Int. Ed.* 2018, 57 (31), 9665–9669.
- (49) Kresse, G.; Furthmüller, J. Efficient Iterative Schemes for Ab Initio Total-Energy Calculations Using a Plane-Wave Basis Set. Phys. Rev. B 1996, 54 (16), 11169–11186.
- (50) Kresse, G.; Furthmüller, J. Efficiency of Ab-Initio Total Energy Calculations for Metals and Semiconductors Using a Plane-Wave Basis Set. Comput. Mater. Sci. 1996, 6 (1), 15–50.
- (51) Blöchl, P. E. Projector Augmented-Wave Method. *Phys. Rev. B* 1994, 50 (24), 17953–17979.
- (52) Kresse, G.; Joubert, D. From Ultrasoft Pseudopotentials to the Projector Augmented-Wave Method. Phys. Rev. B 1999, 59 (3), 1758–1775.
- (53) Perdew, J. P.; Burke, K.; Ernzerhof, M. Generalized Gradient Approximation Made Simple. *Phys. Rev. Lett.* 1996, 77 (18), 3865–3868.
- (54) Grimme, S.; Antony, J.; Ehrlich, S.; Krieg, H. A Consistent and Accurate Ab Initio Parametrization of Density Functional Dispersion Correction (DFT-D) for the 94 Elements H-Pu. J. Chem. Phys. 2010, 132 (15), 154104.
- (55) Pack, J. D.; Monkhorst, H. J. "special Points for Brillouin-Zone Integrations"-a Reply. Phys. Rev. B 1977, 16 (4), 1748–1749.
- (56) Methfessel, M.; Paxton, A. T. High-Precision Sampling for Brillouin-Zone Integration in Metals. *Phys. Rev. B* 1989, 40 (6), 3616–3621
- (57) Henkelman, G.; Uberuaga, B. P.; Jónsson, H. A Climbing Image Nudged Elastic Band Method for Finding Saddle Points and Minimum Energy Paths. J. Chem. Phys. 2000, 113 (22), 9901– 9904.
- (58) Lide, D. R.; Haynes, W. M. M.; Baysinger, G.; Berger, L. I.; Kehiaian, H. V; Roth, D. L.; Zwillinger, D.; Frenkel, M.; Goldberg, R. N. CRC Handbook of Chemistry and Physics 90 Th Edition 2010. 2009, pp 4-144 (refractive index), pp 12-46 (dielectric.)
- (59) Szilvási, T.; Roling, L. T.; Yu, H.; Rai, P.; Choi, S.; Twieg, R. J.; Mavrikakis, M.; Abbott, N. L. Design of Chemoresponsive

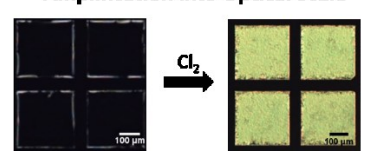
- Liquid Crystals through Integration of Computational Chemistry and Experimental Studies. *Chem. Mater.* **2017**, 3563–3571.
- (60) Tacey, S. A.; Szilvási, T.; Xu, L.; Schauer, J. J.; Mavrikakis, M. The Role of Iron-Oxide Aerosols and Sunlight in the Atmospheric Reduction of Hg(II) Species: A DFT+U Study. Appl. Catal. B Environ. 2018, 234 (15), 347–356.
- (61) Tacey, S. A.; Xu, L.; Szilvási, T.; Schauer, J. J.; Mavrikakis, M. Quantum Chemical Calculations to Determine Partitioning Coefficients for HgCl2 on Iron-Oxide Aerosols. Sci. Total Environ. 2018, 636, 580–587.
- (62) Greeley, J.; Mavrikakis, M. A First-Principles Study of Surface and Subsurface H on and in Ni(111): Diffusional Properties and Coverage-Dependent Behavior. Surf. Sci. 2003, 540 (2–3), 215– 229
- (63) Hunter, J. T.; Pal, S. K.; Abbott, N. L. Adsorbate-Induced Ordering Transitions of Nematic Liquid Crystals on Surfaces Decorated with Aluminum Perchlorate Salts. ACS Appl. Mater. Interfaces 2010, 2 (7), 1857–1865.
- (64) Thomas, S. W.; Vella, S. J.; Dickey, M. D.; Kaufman, G. K.; Whitesides, G. M. Controlling the Kinetics of Contact Electrification with Patterned Surfaces Samuel. *J. Am. Chem. Soc.* 2009, *131* (25), 8746–8747.
- (65) Miller, D. S.; Carlton, R. J.; Mushenheim, P. C.; Abbott, N. L. Introduction to Optical Methods for Characterizing Liquid Crystals at Interfaces. *Langmuir* 2013, 29 (10), 3154–3169.
- (66) ROBERTSON, J. M. The Optical Properties of Organic Compounds. Nature 1944, 154 (3907), 349–350.
- (67) Hunter, J. T.; Abbott, N. L. Dynamics of the Chemo-Optical Response of Supported Films of Nematic Liquid Crystals. Sensors Actuators, B Chem. 2013, 183, 71–80.
- (68) Briggs, D. Handbook of X-Ray Photoelectron Spectroscopy. Surf. Interface Anal. 1981, 3 (4).
- (69) Frey, B. L.; Corn, R. M.; Weibel, S. C. Polarization-Modulation Approaches to Reflection-Absorption Spectroscopy. In Handbook of Vibrational Spectroscopy; Griffiths, P. R., Ed.; John Wiley & Sons, Ltd: Chichester, UK, UK, 2006.
- (70) Liu, W.; Ruiz, V. G.; Zhang, G.-X.; Santra, B.; Ren, X.; Scheffler, M.; Tkatchenko, A. Structure and Energetics of Benzene Adsorbed on Transition-Metal Surfaces: Density-Functional Theory with van Der Waals Interactions Including Collective Substrate Response. New J. Phys. 2013, 15 (5), 053046.
- (71) Santiago-Rodríguez, Y.; Herron, J. A.; Curet-Arana, M. C.; Mavrikakis, M. Atomic and Molecular Adsorption on Au(111). Surf. Sci. 2014, 627 (2), 57–69.
- (72) Nuzzo, R. G.; Fusco, F. A.; Allara, D. L. Spontaneously Organized Molecular Assemblies. 3. Preparation and Properties of Solution Adsorbed Monolayers of Organic Disulfides on Gold Surfaces. J. Am. Chem. Soc. 1987, 109 (8), 2358–2368.
- (73) Chidsey, C. E. D.; Loiacono, D. N.; Sleator, T.; Nakahara, S. STM Study of the Surface Morphology of Gold on Mica. Surf. Sci. 1988, 200 (1), 45–66.
- (74) Hou, Z.; Dante, S.; Abbott, N. L.; Stroeve, P. Self-Assembled Monolayers on (111) Textured Electroless Gold. **1999**, *83* (111), 3011–3014.
- (75) Buffeteau, T.; Desbat, B.; Turlet, J.-M. FTIR Spectroscopy of Monolayers and Ultrathin Films Using Polarization Modulation. *Microchim. Acta* 1988, 95 (1), 23–26.
- (76) Hoffmann, F. M. Infrared Reflection-Absorption Adsorbed Molecules Spectroscopy. Surf. Sci. Rep. 1983, 3, 107–192.
- (77) Karabacak, M.; Cinar, Z.; Kurt, M.; Sudha, S.; Sundaraganesan, N. FT-IR, FT-Raman, NMR and UV-Vis Spectra, Vibrational Assignments and DFT Calculations of 4-Butyl Benzoic Acid. Spectrochim. Acta Part A Mol. Biomol. Spectrosc. 2012, 85 (1), 170–189
- (78) Krishnakumar, V.; Mathammal, R. Density Functional and Experimental Studies on the FT-IR and FT-Raman Spectra and Structure of Benzoic Acid and 3,5-Dichloro Salicylic Acid. J. Raman Spectrosc. 2009, 40 (3), 264–271.
- (79) Han, S. W.; Joo, S. W.; Ha, T. H.; Kim, Y.; Kim, K. Adsorption Characteristics of Anthraquinone-2-Carboxylic Acid on Gold. J. Phys. Chem. B 2002, 104 (50), 11987–11995.
- (80) Wang, J.; Selloni, A. First Principles Study of Fatty Acid Monolayers on Au (111) †. 2009, No. 111, 8895–8900.

- (81) O'Connor, C. R.; Hiebel, F.; Chen, W.; Kaxiras, E.; Madix, R. J.; Friend, C. M. Identifying Key Descriptors in Surface Binding: Interplay of Surface Anchoring and Intermolecular Interactions for Carboxylates on Au(110). Chem. Sci. 2018, 9 (15), 3759-
- (82)Spencer, N. D.; Lambert, R. M. Chlorine Chemisorption and Surface Chloride Formation on Au(111). Surf. Sci. 1981, 107 (1), 237-248.
- (83) Kuca, K.; Pohanka, M. Chemical Warfare Agents. EXS 2010, 100, 543-558.
- (84)Szinicz, L. History of Chemical and Biological Warfare Agents. Toxicology 2005, 214 (3), 167-181.
- (85)Ganesan, K.; Raza, S. K.; Vijayaraghavan, R. Chemical Warfare Agents. J. Pharm. Bioallied Sci. 2010, 2 (3), 166-178.
- (86) https://www.osha.gov/dts/sltc/methods/inorganic/id101/id101. pdf.
- (87)Namba, K.; Ogura, S.; Ohno, S.; Di, W.; Kato, K.; Wilde, M.; Pletikosić, I.; Pervan, P.; Milun, M.; Fukutani, K. Acceleration of Hydrogen Absorption by Palladium through Surface Alloving with Gold. Proc. Natl. Acad. Sci. 2018, 115 (31), 7896-7900.
- (88) Kaichev, V. V.; Prosvirin, I. P.; Bukhtiyarov, V. I.; Unterhalt, H.; Rupprechter, G.; Freund, H. J. High-Pressure Studies of CO Adsorption on Pd(111) by X-Ray Photoelectron Spectroscopy and Sum-Frequency Generation. J. Phys. Chem. B 2003, 107 (15), 3522-3527.
- (89)Carrasco, E.; Aumer, A.; Brown, M. A.; Dowler, R.; Palacio, I.; Song, S.; Sterrer, M. Infrared Spectra of High Coverage CO Adsorption Structures on Pt(111). Surf. Sci. 2010, 604 (15-16), 1320-1325.
- (90)Sinfelt, J. H. Bimetallic Catalysts: Discoveries, Concepts, and Applications; Wiley-Interscience, 1983.
- (91) Rodriguez, J. A.; Goodman, D. W. The Nature of the Metal-Metal

#### **Atomic Scale Elementary Surface Reactions**



#### **Amplification into Optical Scale**



- Bond in Bimetallic Surfaces. Science 1992, 257 (5072), 897-903. Szilvási, T.; Bao, N.; Yu, H.; Twieg, R. J.; Mavrikakis, M.;
- (92)Abbott, N. L. The Role of Anions in Adsorbate-Induced Anchoring Transitions of Liquid Crystals on Surfaces with Discrete Cation Binding Sites. Soft Matter 2018, 14 (5), 797–805.
- (93)Yu, H.; Szilvási, T.; Rai, P.; Twieg, R. J.; Mavrikakis, M.; Abbott, N. L. Computational Chemistry-Guided Design of Selective Chemoresponsive Liquid Crystals Using Pyridine and Pyrimidine Functional Groups. Adv. Funct. Mater. 2018, 1703581.
- (94)Plutschack, M. B.; Pieber, B.; Gilmore, K.; Seeberger, P. H. The Hitchhiker's Guide to Flow Chemistry. Chem. Rev. 2017, 117 (18), 11796-11893.
- (95)Wegner, J.; Ceylan, S.; Kirschning, A. Flow Chemistry - A Key Enabling Technology for (Multistep) Organic Synthesis. Adv. Synth. Catal. 2012, 354 (1), 17-57.
- (96)Pérez-Mitta, G.; Tuninetti, J. S.; Knoll, W.; Trautmann, C.; Toimil-Molares, M. E.; Azzaroni, O. Polydopamine Meets Solid-State Nanopores: A Bioinspired Integrative Surface Chemistry Approach to Tailor the Functional Properties of Nanofluidic Diodes. J. Am. Chem. Soc. 2015, 137 (18), 6011-6017.
- (97)Fang, R.; Zhang, H.; Yang, L.; Wang, H.; Tian, Y.; Zhang, X.; Jiang, L. Supramolecular Self-Assembly Induced Adjustable Multiple Gating States of Nanofluidic Diodes. J. Am. Chem. Soc. 2016, 138 (50), 16372-16379.

#### SUPPORTING INFORMATION

# Amplification of Elementary Surface Reaction Steps on Transition Metal Surfaces using Liquid Crystals: Dissociative Adsorption and Dehydrogenation

Huaizhe Yu<sup>†,+</sup>, Tibor Szilvási<sup>‡,+</sup>, Kunlun Wang<sup>#</sup>, Jake I. Gold<sup>‡</sup>, Nanqi Bao<sup>†</sup>, Robert J. Twieg<sup>#</sup>, Manos Mavrikakis<sup>\*,‡</sup> and Nicholas L. Abbott<sup>\*,†</sup>

<sup>†</sup>Robert Frederick Smith School of Chemical and Biomolecular Engineering, Cornell University, 1 Ho Plaza, Ithaca, New York 14853, United States

<sup>‡</sup>Department of Chemical and Biological Engineering, University of Wisconsin-Madison, 1415 Engineering Drive, Madison, Wisconsin 53706, United States

\*Department of Chemistry and Biochemistry, Kent State University, 1175 Risman Drive, Kent, Ohio 44242, United States

<sup>+</sup>H.Y. and T.S. contributed equally to this work.

#### 1. Computational methods

#### Calculation of phase diagram for Cl adsorption on Au(111)

We built on the approach described by Bollinger et al<sup>1</sup> and Xu et al<sup>2</sup>. We calculated the grand potential per surface area  $(\Omega)$  for the Cl adlayer at each investigated surface coverage:

$$\Omega(p,T) = [G_{nCl+substrate} - G_{substrate} - n\mu_{Cl*}]/A$$

where  $G_{nCl+substrate}$  is the Gibbs free energy of the Cl covered Au(111),  $G_{substrate}$  is the Gibbs free energy of clean Au(111),  $\mu_{Cl^*}$  is the chemical potential of adsorbed Cl ('\*' denotes adsorption), n is the number of adsorbed Cl atoms, and A is surface area of the unit cell. We assumed equilibrium between the gas phase and the surface, and thus the chemical potential of adsorbed Cl is equal to the chemical potential of ½ Cl<sub>2</sub>(g) ( $\mu_{Cl^*} = 1/2$   $\mu_{Cl2}$ ).  $\mu_{Cl2}$  can be expressed as

$$\mu_{Cl2}(p,T) = H_{Cl2}(p_0,T) - TS_{Cl2}(p_0,T) + kT \ ln(p/p_0)$$

$$\mu_{Cl2}(p,T) = E_{Cl2} + \left[H_{Cl2}(p_0,T=0\ K) - E_{Cl2}\right] + \left[H_{Cl2}(p_0,T) - H_{Cl2}(p_0,T=0\ K)\right] - TS_{Cl2}(p_0,T) + kT\ ln(p/p_0)$$

where  $E_{\text{Cl2}}$  is the total energy of a  $\text{Cl}_2$  molecule in the gas phase,  $H_{\text{Cl2}}(p_0, T=0 \text{ K})$  is the enthalpy of  $\text{Cl}_2(g)$  at standard pressure  $p_0$  (101325 Pa) and 0 K,  $H_{\text{Cl2}}(p_0, T)$  is the enthalpy of  $\text{Cl}_2(g)$  at standard pressure  $p_0$  (101325 Pa) and temperature T, and  $S_{\text{Cl2}}(p_0, T)$  is the entropy of  $\text{Cl}_2$ , while  $[H_{\text{Cl2}}(p_0, T=0 \text{ K}) - E_{\text{Cl2}}]$  is the zero-point energy of  $\text{Cl}_2$  and  $[H_{\text{Cl2}}(p_0, T) - H_{\text{Cl2}}(p_0, T=0 \text{ K})]$  is the temperature dependence of  $\text{Cl}_2$  enthalpy. Thermodynamic correction terms ( $[H_{\text{Cl2}}(p_0, T=0 \text{ K}) - E_{\text{Cl2}}]$ ,  $[H_{\text{Cl2}}(p_0, T) - H_{\text{Cl2}}(p_0, T=0 \text{ K})]$ , and  $S_{\text{Cl2}}(p_0, T)$ ) were calculated directly from analysis of the vibrational, rotational, and translational degrees of freedom of a  $\text{Cl}_2$  molecule in vacuum.

 $G_{nCl+substrate}$  and  $G_{substrate}$  can be expressed similarly to  $\mu_{Cl2}(p,T)$ , however we neglected the pressure dependence of  $G_{nCl+substrate}$  and  $G_{substrate}$  and the vibrational contribution of the substrate to the thermodynamic correction terms. Both assumption are justified because previous analyses showed the relatively small contribution of these terms, and additionally, error cancellation is expected to further reduce the error originating from these assumptions. Accordingly,

 $G_{nCl+substrate} = E_{nCl+substrate} + \left[H_{nCl+substrate}\left(T=0\ K\right) - E_{nCl+substrate}\right] + \left[H_{nCl+substrate}(T) - H_{nCl+substrate}(T=0\ K)\right] - TS_{nCl+substrate}(T)$  where  $E_{nCl+substrate}$  is the energy of the Cl covered Au(111),  $H_{nCl+substrate}(T=0\ K)$  is the enthalpy of the Cl covered Au(111) at zero temperature,  $H_{nCl+substrate}(T)$  is the enthalpy of the Cl covered Au(111) at temperature

T, and  $S_{nCl+substrate}(T)$  is the entropy of the Cl covered Au(111) at temperature T, while  $[H_{nCl+substrate}(T=0\ K)-E_{nCl+substrate}]$  is the zero point energy contribution of the Cl overlayer on Au(111) and  $[H_{nCl+substrate}(T)-H_{nCl+substrate}(T=0\ K)]$  is the temperature dependence of the enthalpy of the Cl overlayer on Au(111). Thermodynamic correction terms,  $[H_{nCl+substrate}(T=0\ K)-E_{nCl+substrate}]$ ,  $[H_{nCl+substrate}(T)-H_{nCl+substrate}(T=0\ K)]$ , and  $S_{nCl+substrate}(T)$ , were calculated from the analysis of the vibrational, rotational, and translational degrees of freedom of the Cl overlayer on Au(111). Additionally, because of the abovementioned assumptions,  $G_{substrate}=E_{substrate}$ .

We evaluated 1/3, 4/9, 1/2, 5/9, and 2/3 ML Cl coverages on Au(111) to construct the phase diagram. Our choice for different surface coverages was motivated by previous experimental studies confirmed the presence of 1/3 ML Cl coverage on Au(111) in ultra-high vacuum (UHV) experiments.<sup>3,4</sup> Additionally, in our experimental setup, the Cl<sub>2</sub> partial pressure is above 0.1 Pa, which is at least six orders of magnitude higher than that in UHV experiments. We note that previous works suggested that high Cl<sub>2</sub> partial pressure can indeed induce further Cl adsorption, resulting in higher than 1/3 ML coverages, but the resulting overlayer structures and potential reconstructions of the surface are still unclear.<sup>3,4</sup> For this initial study, we neglected the potential reconstruction of the surface, and we only investigated Au(111) surfaces. We found that the optimal Cl coverage under our experimental conditions (ambient temperature and 1 ppm Cl<sub>2</sub>) is ½ ML Cl coverage. Figure S1 shows the obtained most favorable ½ ML Cl covered Au(111) surface. All Cl atoms occupy bridge sites, each Cl atom having two neighboring Au atoms, while all surface Au atoms have only one Cl adsorbate.

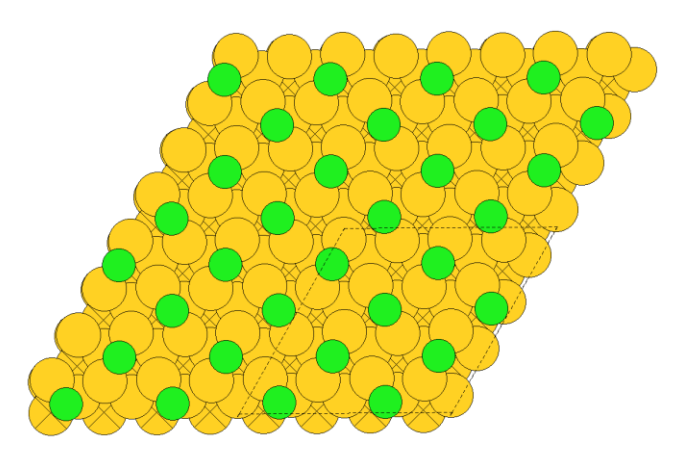


**Figure S1**. Calculated structure of ½ ML Cl covered Au(111) surface. Green and yellow colors indicate Cl and Au atoms, respectively. Crossed atoms were not allowed to relax not moved during energy minimization. Dashed lines indicate the unit cell borders. Multiple unit cells are shown to recognize surface pattern of Cl adatoms.

## 2. Synthesis

# Synthesis of 4'-cyanobiphenyl-4-carboxylic acid (CBCA, Scheme 1).5

A 100 ml round bottom flask fitted with a magnetic stir bar was charged with 4-bromobenzoic acid (2.01, 10.0 mmol) and a mixed solvent comprising  $H_2O$  (6.0 ml), 1,4-dioxane (15.0 ml) and  $Pd(PPh_3)_4$  (115 mg, 1.0 mol%). To this suspension was added 4-cyanophenylboronic acid (1.70 g, 15.0 mmol, 1.5 equiv.) and potassium carbonate (2.76 g, 20.0 mmol, 2.0 equiv.). This mixture was refluxed and the reaction was monitored by thin layer chromatography (TLC) until completion. After cooling to room temperature, the mixture was filtered through a Celite pad and the pad was washed with a 1:1 mixture of  $H_2O$ /methanol (400 ml). The filtrate was then acidified with 10% hydrochloric acid dropwise until pH = 4-4.5. The precipitate

was collected by vacuum filtration and washed with water. The crude product was then recrystallized from methanol to afford white crystals (1.1 g, 50%). K 268 N 315 I (ref. K 266 N 315 I<sup>6</sup>) <sup>1</sup>H NMR (DMSO-d<sub>6</sub>, 400 MHz) δ (ppm): 13.13 (s, 1H), 8.05 (m, 2H), 7.98 (m, 4H), 7.91 (m, 2H).

# Synthesis of 4'-cyanobiphenyl-4-carboxylic methyl ester (CBCM).<sup>7</sup>

In a 50 ml round bottom flask fitted with a magnetic stir bar, 4'-cyanobiphenyl-4-carboxylic acid (400 mg) was dissolved in methanol (20.0 ml) followed by the addition of a catalytic amount of concentrated sulfuric acid. The resulting mixture was stirred at reflux overnight. TLC analysis indicated that the starting acid was consumed. The reaction was cooled, and the precipitate was filtered by vacuum to give a white solid. This crude product was then recrystallized from ethanol to afford white crystals (330 mg, 78%). GC-MS: 237.13 found 237.25 calc.  $^{1}$ H NMR (CDCl<sub>3</sub>, 400 MHz)  $\delta$  (ppm): 8.13 (m, 2H), 7.75 (m, 2H), 7.72 (m, 2H), 7.66 (m, 2H), 3.95 (s, 3H);  $^{13}$ C NMR (CDCl<sub>3</sub>, 100 MHz)  $\delta$  (ppm): 166.6, 144.4, 143.4, 132.7, 130.4, 130.2, 127.9, 127.3, 118.7, 111.8, 52.3.

# Synthesis of sodium 4'-cyanobiphenyl-4-carboxylate (CBCNa).8

In a 50 ml round bottom flask fitted with a magnetic stir bar, 4'-cyanobiphenyl-4-carboxylic acid (446 mg, 2.0 mmol) was dissolved in ethanol (10.0 ml). To the resulting suspension was added a solution of t-BuONa (192 mg, 2.0 mmol) in 10.0 ml ethanol dropwise. Once the addition was complete, the resulting mixture was stirred at room temperature overnight. The precipitate was filtered by vacuum and washed with ethanol (3 x 5.0 ml) and diethyl ether (3 x 5.0 ml). The desired product was then obtained as an off-white solid (410 mg, 84%). MP>300 °C.  $^{1}$ H NMR (DMSO-d<sub>6</sub>, 400 MHz)  $\delta$  (ppm): 7.96 (d, J = 8.0 Hz, 2H), 7.90 (m, 4H), 7.65 (d, J = 8.0 Hz, 2H);  $^{13}$ C NMR (DMSO-d<sub>6</sub>, 100 MHz)  $\delta$  (ppm): 169.1, 145.3, 141.9, 138.4, 133.3, 130.2, 128.0, 126.3, 119.4, 110.2.

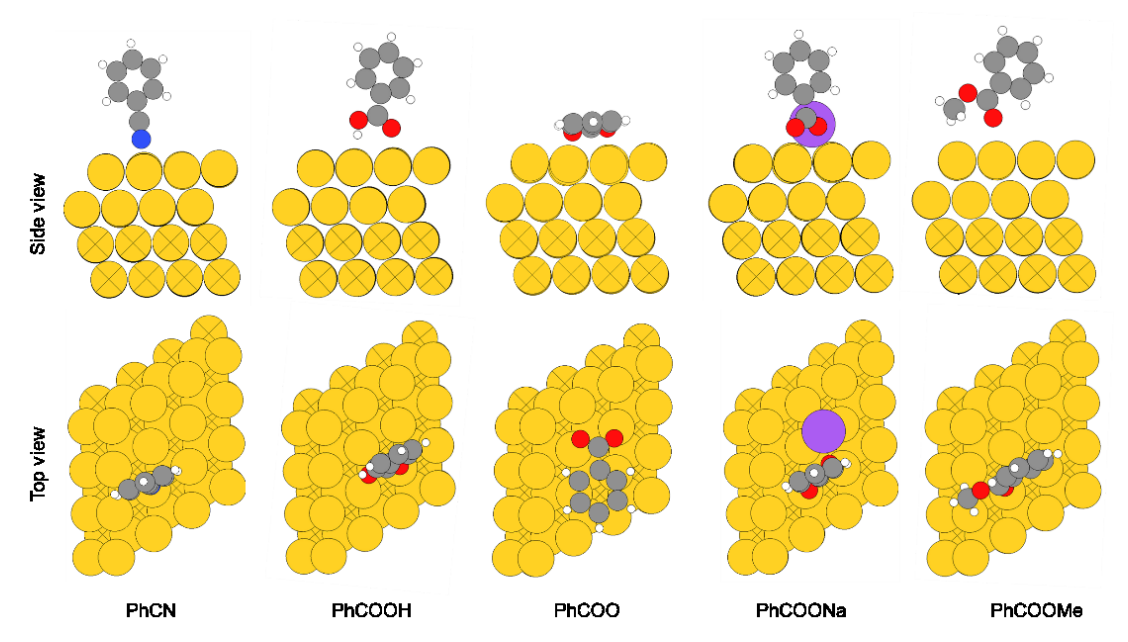


**Figure S2**. Minimum energy, but *not* the most preferred structures, for PhCN, PhCOOH, PhCOO, PhCOONa and PhCOOMe on Au(111) slab. White, grey, blue, red, purple and yellow colors indicate H, C, N, O, Na and Au atoms, respectively. Crossed Au (yellow) atoms were kept fixed during geometry optimization.

#### 3. Additional discussion.

# Analysis of the orientation of PhCN on Cl covered Au(111)

We investigated the binding properties of PhCN on Cl covered Au(111) by evaluating the binding energy of PhCN in perpendicular and parallel orientations. We applied 1/3 ML Cl coverage in a 3x3 unit cell of Au(111). We found that PhCN binding in parallel orientation is -0.72 eV (Figure S3a) while in perpendicular orientation is -0.39 eV (Figure S3b). Thus we predict that parallel orientation is still preferred on Cl covered Au(111) surface similar to clean Au(111). We also note that higher than 1/3 ML Cl coverage is expected to behave similarly.

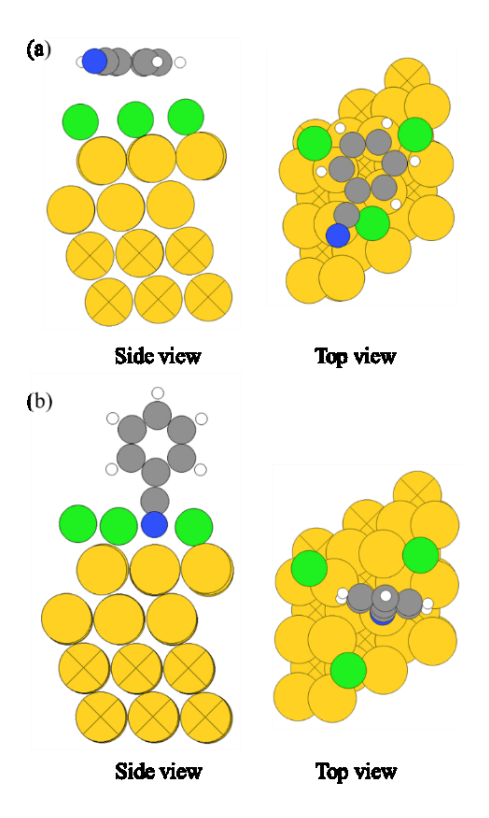


**Figure S3.** Calculated structure of PhCN on 1/3 monolayer Cl pre-covered Au(111) surface in (a) parallel and (b) perpendicular orientation. White, grey, green, red, and yellow colors indicate H, C, Cl, O and Au atoms, respectively. Crossed atoms were not allowed to relax not moved during energy minimization.

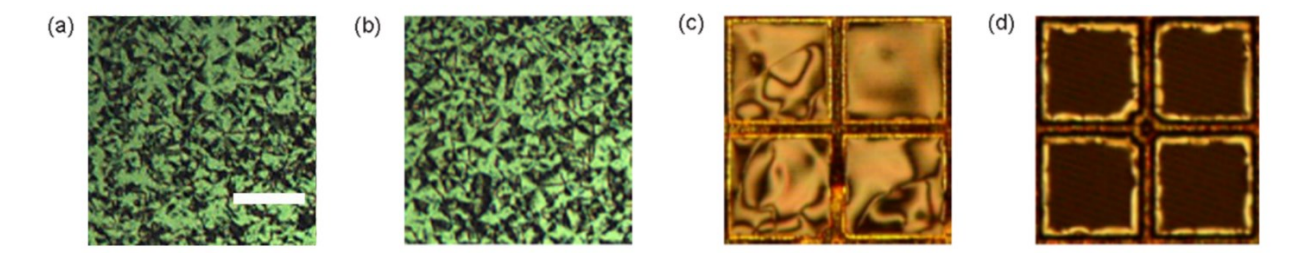


**Figure S4**. Optical micrographs (crossed polars) of (a) 5CB sandwiched between two gold films, (b) CBCA-5CB ( $C_{CBCA} = 0.1 \text{ mol}\%$ ) sandwiched between two borosilicate surfaces, (c) CBCA-5CB ( $C_{CBCA} = 0.1 \text{ mol}\%$ ) on Si surface, (d) CBCA-5CB ( $C_{CBCA} = 0.1 \text{ mol}\%$ ) on gold surface deposited on Si surface. Scale bar in (a): 100 µm.

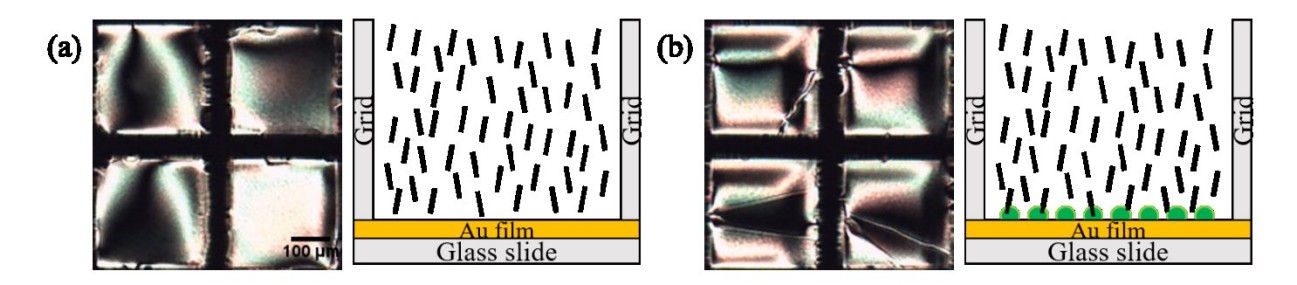


**Figure S5**. Optical micrographs (crossed polars) of 5CB films on Au surface exposed to 1 ppm  $Cl_2$  at (a) 0 min (b) 30 mins. A schematic representation of the LCs is shown to the side of each optical image. Green circles indicate the adsorbed Cl atoms. Black lines indicate the director of LCs. Scale bar: 100  $\mu$ m.

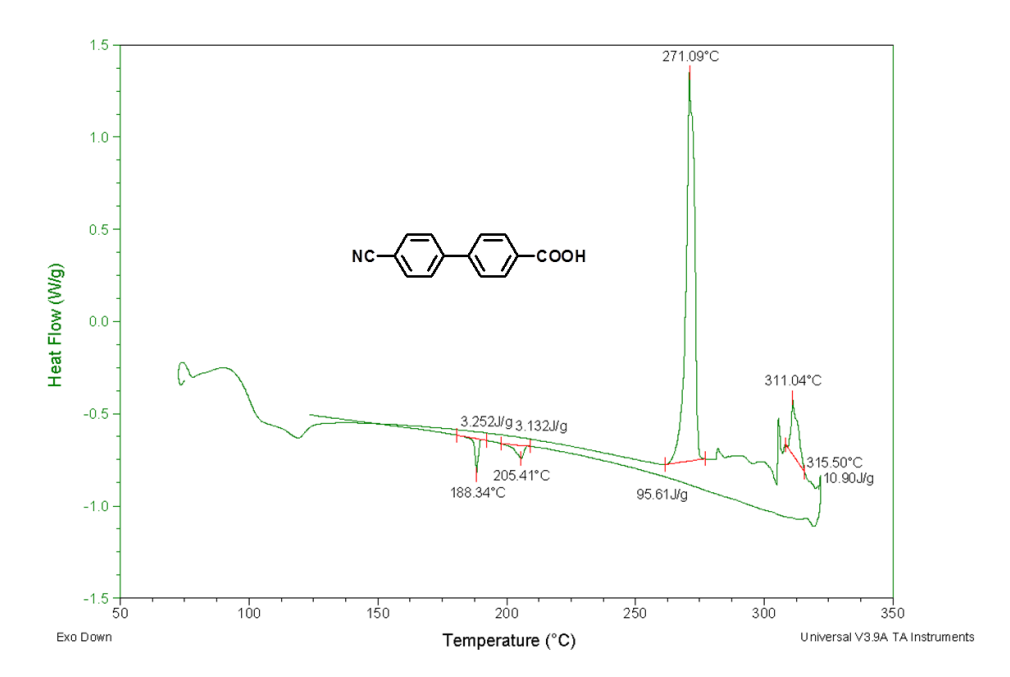


Figure S6. Differential Scanning Calorimetry (DSC) for CBCA.



Figure S7. Optical micrographs (crossed polars) for CBCA at 314 °C.

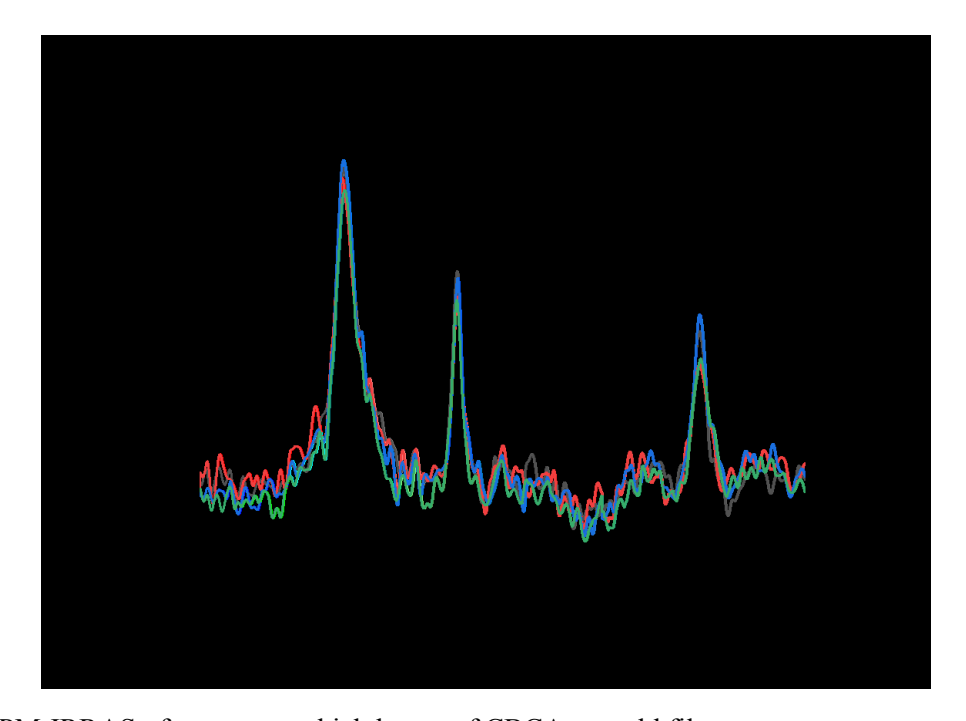


Figure S8. PM-IRRAS of nanometer-thick layers of CBCA on gold films.

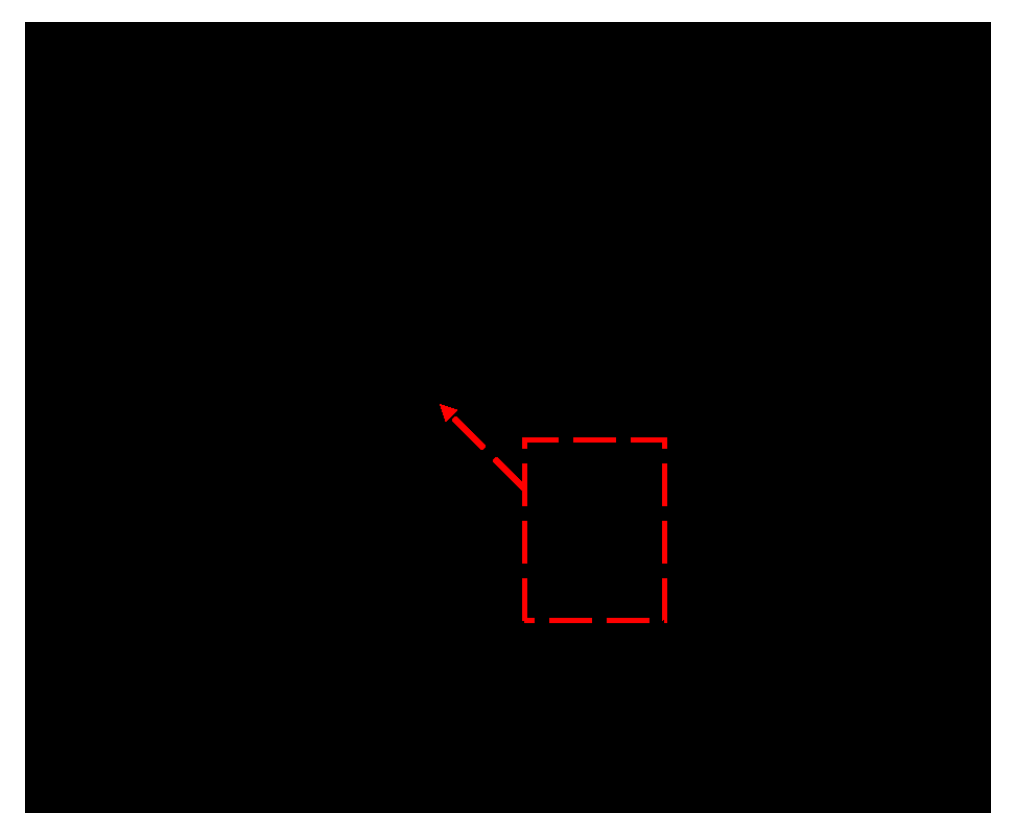
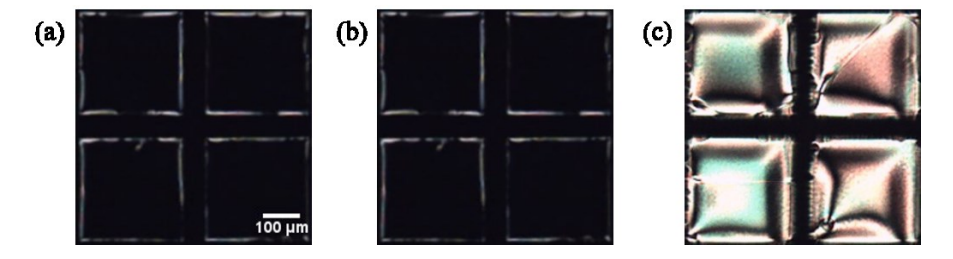


Figure S9. XPS characterization of gold films.



**Figure S10**. Optical micrographs (crossed polars) of LC films comprising CBCA-5CB of (a)  $C_{CBCA} = 0.005$  mol%, (b)  $C_{CBCA} = 0.002$  mol% and (c)  $C_{CBCA} = 0.001$  mol% on a gold surface. Scale bar: 100  $\mu$ m.

### Evaluation of the CBCA coverage on gold surface

We first start our evaluation of the relative surface coverage of 5CB and CBCA-derived carboxylate on Au(111) by calculating equilibrium constant based on their relative BE. We calculate BE of PhCN and PhCOO, surrogates of 5CB and CBCA-derived carboxylate, to be -0.91 and -1.15 eV (Table 1), respectively. The difference between the BE of PhCN and PhCOO is 0.24 eV in favor of PhCOO, which indicates the dominance of PhCOO on the surface as 0.06 eV difference in BE results in one order of magnitude difference in equilibrium constant at room temperature. Using the binding energy listed above and Table 1, we estimate the equilibrium constant of the process PhCOO + PhCN-Au → PhCN + PhCOO-Au by

neglecting the entropy change. By solving the following equation,  $\Delta G = BE_{PhCN} - BE_{PhCOO} = -k_BT \ln K$ , we calculate the equilibrium constant to be  $K = 1.1 \times 10^4$ . With this large equilibrium constant, we expect that almost all the CBCA molecules in the LC mixture will adsorb on the Au surface by replacing 5CB. Thus, we calculate an equilibrium constant of  $1.1 \times 10^4$  from the BE difference, suggesting complete coverage of PhCOO on Au(111) based on thermodynamic arguments.

To further elucidate on the coverage of CBCA-derived carboxylate in our experimental setup, we estimate the total number of CBCA molecules and exposed gold atoms in a square pore of a TEM grid, which is used as a container of LC film in our experiments (see description in Materials section) and shown in Figure 6a, S2, and S3. We calculate the total surface area of gold to be  $8.12 \times 10^{10}$  nm² in a  $285 \mu m \times 285 \mu m$  square pore. If we assume the most stable Au(111) surface for the whole gold surface, which should be the dominant surface facet, DFT calculations suggest that a (3x3) unit cell with 9 surface atoms covers 0.66 nm². Thus, there are  $1.10 \times 10^{12}$  gold atoms exposed on the gold surface in a square pore. From the volume of the square pore  $(1.46 \times 10^{-6} \text{ mL})$ , we can calculate the total number of CBCA molecules in a square pore to be  $7.11 \times 10^{10}$  using the average molecular weight of 5CB (249.36 g/mol), the density of the LC mixture (1.008 g/mL) and the concentration of CBCA (0.002 mol%). Therefore, if we assume that all CBCA molecules are on the surface, we calculate a  $7.11 \times 10^{10}/1.10 \times 10^{12} = 0.07$  ML surface coverage of CBCA-derived carboxylate.

Overall, we conclude that CBCA-derived carboxylate should cover the gold surface because of the large equilibrium constant, but the total amount of CBCA-derived carboxylate is so low in the experiments with 0.002 mol% CBCA that even when all CBCA are segregated to the surface, they can only form a submonolayer coverage.

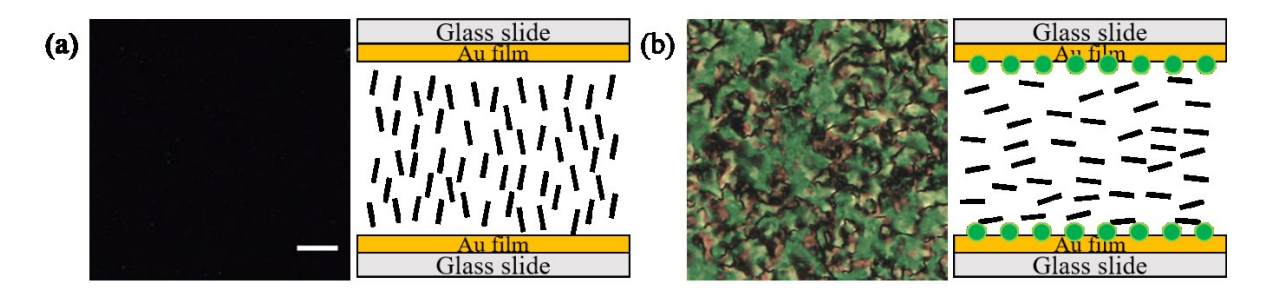


**Figure S11**. Optical micrographs (crossed polars) of LC films comprising of (a)  $Cl_2$  exposed CBCA-5CB ( $C_{CBCA} = 0.002 \text{ mol}\%$ ) supported on gold surface and (b) CBCA-5CB ( $C_{CBCA} = 0.002 \text{ mol}\%$ ) supported on  $Cl_2$ -absorbed gold surface. A schematic representation of the LCs is shown to the side of each optical image. Black lines indicate the director of LCs. Green circles represent Cl atoms. Scale bar: 100  $\mu$ m.

**Table S1.** T<sub>NI</sub> of 5CB-CBCA mixtures before and after exposed to a gaseous 1 ppm Cl<sub>2</sub>

C <sub>CBCA</sub> in 5CB (mol%)	0	0.002	0.005
T <sub>NI</sub> before exposure (°C)	35.5	35.5	35.5
T <sub>NI</sub> at 60 mins (°C)	35.5	35.5	35.5

Evaluation of the orientation of thin film of pure CBCA supported on a gold film after exposure to Cl<sub>2</sub>. We exposed a thin film (~2nm) of pure CBCA supported on a gold film to a nitrogen stream containing 1 ppm Cl<sub>2</sub> for 30 mins at 80 °C. After exposure, we found the infrared spectrum to be indistinguishable from Figure 3b, I and 3d, I. This result reveals that a monolayer of pure CBCA does not react and reorganize with Cl<sub>2</sub> in the same way as mixed films of 5CB and CBCA supported on gold. We note that the melting temperature of pure CBCA is much higher than the CBCA and 5CB mixture used in the experiments reported in the main text.

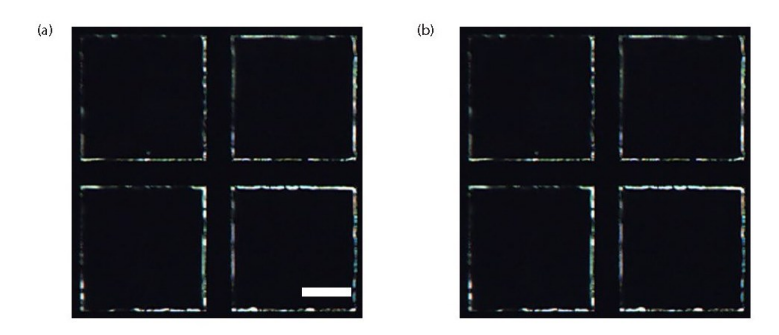


**Figure S12**. Optical micrographs (crossed polars) of LCs comprising of 5CB-CBCA ( $C_{CBCA} = 0.002 \text{ mol}\%$ ) (a) before exposure and (b) after exposure to a vapor of 80% RH N<sub>2</sub>, 5 ppm NH<sub>3</sub>, 5 ppm DMMP or 5 ppm Ethylene oxide for 1 hour. Scale bar: 100  $\mu$ m.

**Table S2.** Binding energy of different interfering agents on clean Au(111) using a (4x4) unit cell. All energies are in eV. Binding energy is defined relative to the gas-phase energy of the identical molecule (see details in Methods). Note that the binding energy of CBCA-derived carboxylate is -1.15 eV in 1/16 coverage.

Molecule	Perpendicular	Coverage
N <sub>2</sub>	-0.11	1/16
DMMP	-0.61	1/16
$NH_3$	-0.59	1/16
Ethylene- oxide	-0.40	1/16
НСНО	-0.32	1/16

#### Other principles for Cl<sub>2</sub> detection

Previous studies have reported various principles and devices for the detection of chlorine gas. For example, metal oxide-based sensors, such as CdSnO<sub>3</sub><sup>9</sup>, In<sub>2</sub>O<sub>3</sub><sup>10</sup> and ZnO<sup>11</sup>, have been reported to detect chlorine gas

below 1 ppm. However, these require operation at temperatures above 100 °C. In contrast, a Sb-doped SnO<sub>2</sub> sensor<sup>11</sup> has been reported to detect chlorine gas at room temperature, but it failed to detect chlorine gas below 1 ppm. Additionally, traditional sensors are expensive and not well-suited to use as wearable devices for measurement of human exposure to chemical environments.

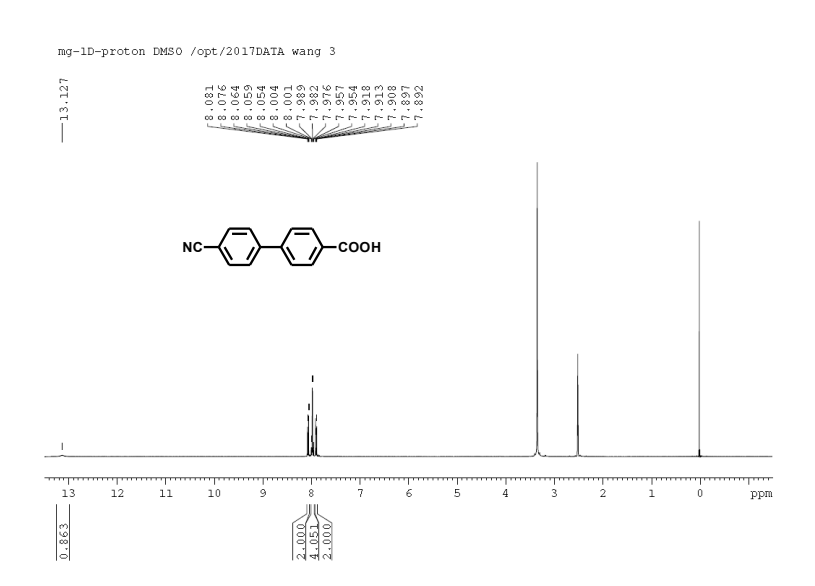


Figure S13. <sup>1</sup>H NMR spectrum of CBCA.

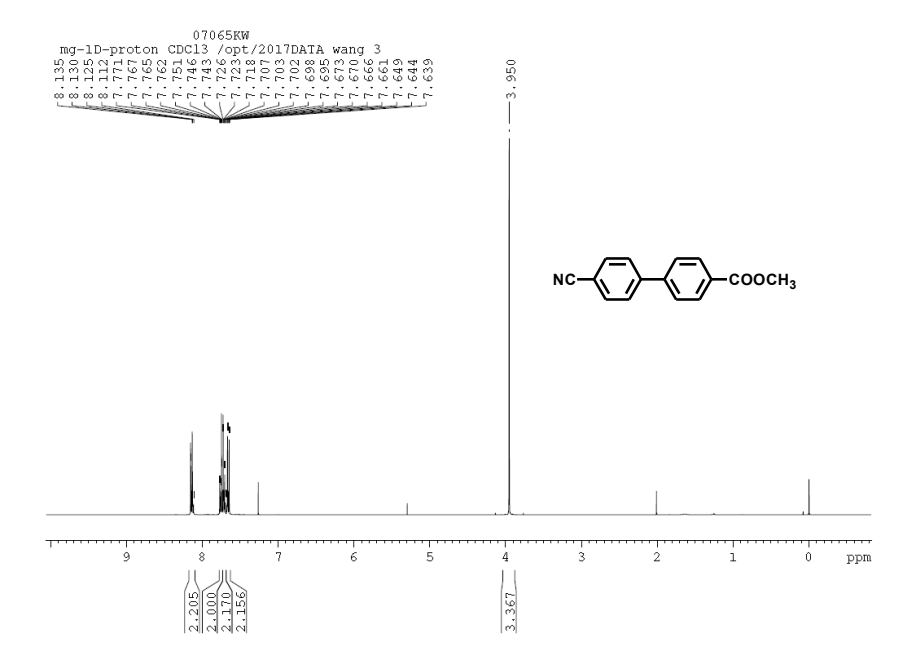


Figure S14. <sup>1</sup>H NMR spectrum of CBCM.

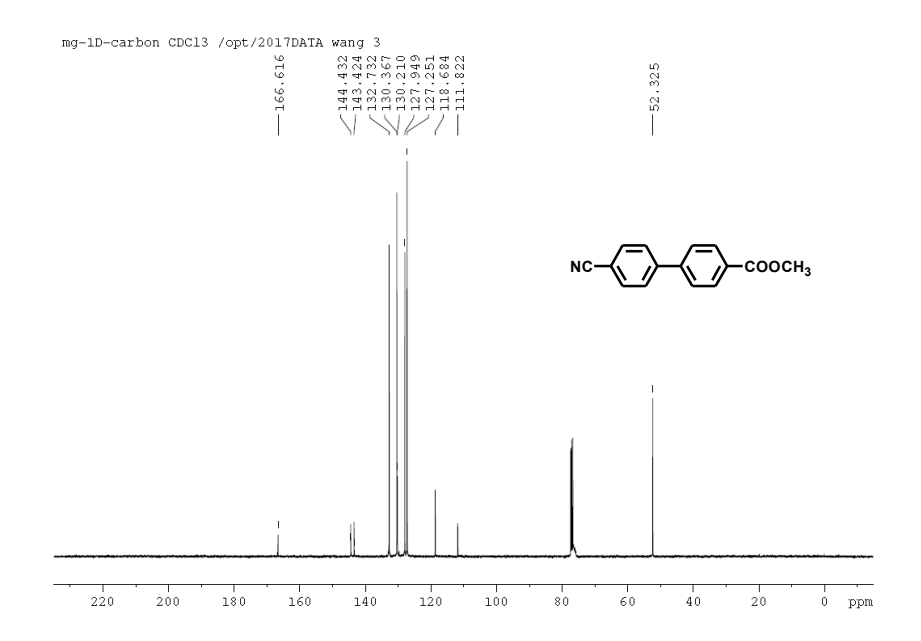


Figure S15. <sup>13</sup>C NMR spectrum of CBCM.

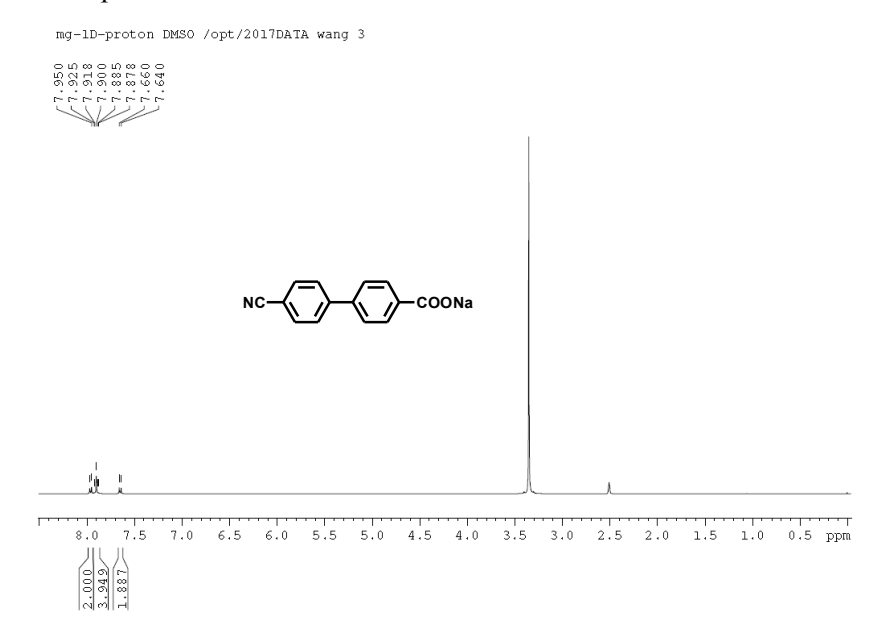


Figure S16. <sup>1</sup>H NMR spectrum of CBCNa.

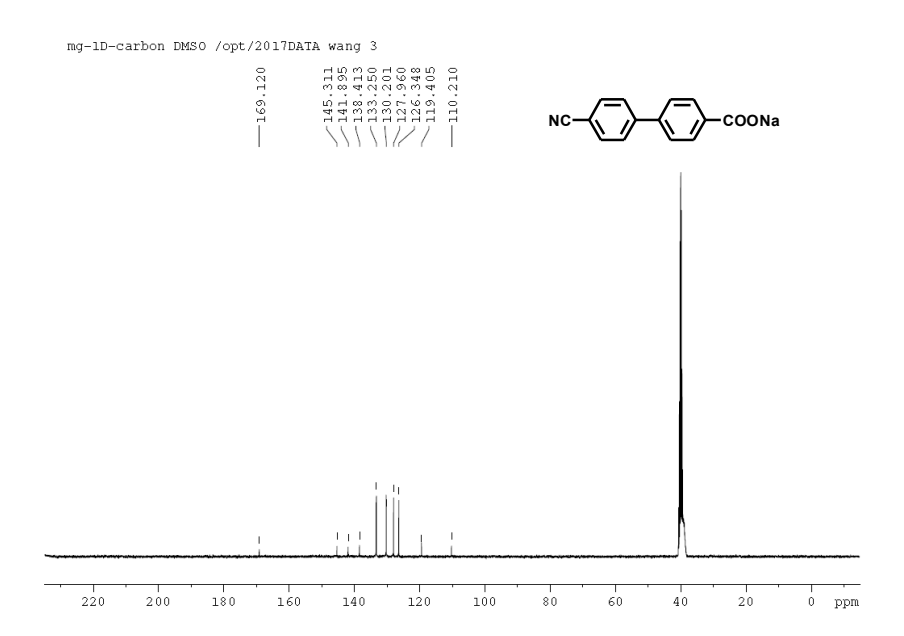


Figure S17.  $^{13}$ C NMR spectrum of CBCNa.

#### References

- (1) Bollinger, M. V; Jacobsen, K. W.; No, J. K.; Mos, E. Atomic and Electronic Structure of MoS2 Nanoparticles. **2003**, No. June 2002, 1–17.
- (2) Xu, L.; Stangland, E. E.; Mavrikakis, M. A DFT Study of Chlorine Coverage over Late Transition Metals and Its Implication on 1,2-Dichloroethane Hydrodechlorination. *Catal. Sci. Technol.* **2018**, 8 (6), 1555–1563.
- (3) Kastanas, G. N.; Koel, B. E. Interaction of Cl2 with the Au(111) Surface in the Temperature Range of 120 to 1000 K. *Appl. Surf. Sci.* **1993**, *64* (3), 235–249.
- (4) Gao, W.; Baker, T. A.; Zhou, L.; Pinnaduwage, D. S.; Kaxiras, E.; Friend, C. M. Chlorine Adsorption on Au(111): Chlorine Overlayer or Surface Chloride? *J. Am. Chem. Soc.* **2008**, *130* (11), 3560–3565.
- (5) Zhang, P.; Bao, L.; Zuckett, J. F.; Goldman, E. A.; Jia, Z. J.; Arfsten, A.; Edwards, S.; Sinha, U.; Hutchaleelaha, A.; Park, G.; et al. Design, Synthesis, and SAR of Anthranilamide-Based Factor Xa Inhibitors Incorporating Substituted Biphenyl P4 Motifs. 2004, 14, 983–987.
- (6) Byron, D. J.; Gray, G. W.; Wilson, R. C. The Synthesis of Some Substituted Biphenyl-4-Carboxylic Acids, 4-Biphenylylacetic Acids, and 4-Aminobiphenyls. J. Chem. Soc. C Org. 1966, No. 840, 840.
- (7) Ananthakrishnanadar, P.; Kannan, N. The Effects of Substituents on the Rate of Saponification of Biphenyl-4-Carboxylates. **1984**, 35–37.
- (8) Goossen, L. J.; Linder, C.; Rodríguez, N.; Lange, P. P. Biaryl and Aryl Ketone Synthesis via Pd-Catalyzed Decarboxylative Coupling of Carboxylate Salts with Aryl Triflates. **2009**, 9336–9349.
- (9) Xiangfeng, C. High Sensitivity Chlorine Gas Sensors Using CdSnO3 Thick Film Prepared by Co-Precipitation Method. *Sensors Actuators B Chem.* **2004**, *98* (2–3), 215–217.
- (10) Tamaki, J.; Niimi, J.; Ogura, S.; Konishi, S. Effect of Micro-Gap Electrode on Sensing Properties to Dilute Chlorine Gas of Indium Oxide Thin Film Microsensors. **2006**, *117*, 353–358.
- (11) Chaparadza, A.; Rananavare, S. B. Room Temperature Cl<sub>2</sub> Sensing Using Thick Nanoporous Films of Sb-Doped SnO<sub>2</sub>. *Nanotechnology* **2008**, *19* (24), 245501.